Spin dependence of K mixing, strong configuration mixing, and electromagnetic properties of ^{178}Hf

A. B. Hayes,[1] D. Cline,[1] C. Y. Wu,[1,2] H. Ai,[3] H. Amro,[3] C. Beausang,[4] R. F. Casten,[3] J. Gerl,[5] A. A. Hecht,[3] A. Heinz,[3] H. Hua,[1,*] R. Hughes,[3] R. V. F. Janssens,[6] C. J. Lister,[6] A. O. Macchiavelli,[7] D. A. Meyer,[3,†] E. F. Moore,[6] P. Napiorkowski,[8] R. C. Pardo,[6] Ch. Schlegel,[5] D. Seweryniak,[6] M. W. Simon,[1] J. Srebrny,[8,9] R. Teng,[1] K. Vetter,[7] and H. J. Wollersheim[5]

[1]*Department of Physics and Astronomy, University of Rochester, Rochester, New York 14627, USA*
[2]*Lawrence Livermore National Laboratory, Livermore, California 94550, USA*
[3]*Wright Nuclear Structure Laboratory, Yale University, New Haven, Connecticut 06520, USA*
[4]*Physics Department, University of Richmond, Richmond, Virginia 23173, USA*
[5]*GSI, Gesellschaft für Schwerionenforschung, Planckstrasse 1, D-64291 Darmstadt, Germany*
[6]*Physics Division, Argonne National Laboratory, Argonne, Illinois 60439, USA*
[7]*Lawrence Berkeley National Laboratory, Berkeley, California 94720, USA*
[8]*Heavy Ion Laboratory, Warsaw University, Warszawa, Poland*
[9]*Institute of Experimental Physics, Warsaw University, Warszawa, Poland*

(Received 16 October 2006; published 16 March 2007)

The combined data of two Coulomb excitation experiments has verified the purely electromagnetic population of the $K^\pi = 4^+, 6^+, 8^-$, and 16^+ rotational bands in ^{178}Hf via $2 \leqslant \nu \leqslant 14$ K-forbidden transitions, quantifying the breakdown of the K-selection rule with increasing spin in the low-K bands. The γ-, 4^+, and 6^+ bands were extended, and four new states in a rotational band were tentatively assigned to a previously known $K^\pi = 0^+$ band. The quasiparticle structure of the 6^+ ($t_{\frac{1}{2}} = 77$ ns) and 8^- ($t_{\frac{1}{2}} = 4$ s) isomer bands were evaluated, showing that the gyromagnetic ratios of the 6^+ isomer band are consistent with a pure $\pi\frac{7}{2}^+[404], \pi\frac{5}{2}^+[402]$ structure. The 8^- isomer band at 1147 keV and the second 8^- band at 1479 keV, thought to be predominantly $\nu\frac{7}{2}^-[514], \nu\frac{9}{2}^+[624]$ and $\pi\frac{9}{2}^-[514], \pi\frac{7}{2}^+[404]$, respectively, are mixed to a degree approaching the strong-mixing limit. Based on measured $\langle K^\pi = 16^+ \| E2 \| K^\pi = 0^+ \rangle$ matrix elements, it was shown that heavy-ion bombardment could depopulate the 16^+ isomer at the $\sim$1% level, although no states were found that would mediate photodeexcitation of the isomer via low-energy x-ray absorption.

DOI: 10.1103/PhysRevC.75.034308 PACS number(s): 27.70.+q, 21.60.Ev, 23.20.Lv, 23.20.−g

I. INTRODUCTION

Nuclei in the $A \approx 180$ region provide opportunities to study the interplay between collective and single-particle behavior in nuclear structure. In recent years, the study of electromagnetic (EM) excitation and deexcitation of high-K isomeric states [1–6] has demonstrated significant violations of the K-selection rule in axially symmetric, quadrupole-deformed nuclei. An earlier Letter [4] showed that K-selection violations in ^{178}Hf are mediated by a rapid increase in the magnitude of the K-forbidden transition matrix elements $\langle K_f | \mathcal{M}\lambda | K_i \rangle$ with increasing spin. The present work shows that the K-mixing occurs primarily in low-K bands, and probes the mixing of high-K components with increasing spin. The quadrupole moments and gyromagnetic ratios g_K and g_R measured from the in-band $E2/M1$ branching ratios can be used to develop a picture of the collective and single-particle properties, revealing admixtures in the wave functions of rotational bands as well as the strength of the mixing. Changes in the moments of inertia of the nucleus provide additional evidence for band mixing, which is compared in the present work with the evolution of EM matrix elements as a function of spin.

Although the results of this work include several aspects of nuclear structure, the concepts and quantities related to the K-quantum number and its conservation require a more detailed introduction. If a deformed nucleus has axial symmetry, then K, the projection of the total spin I on the symmetry axis, is a good quantum number, and the K-selection rule [7] forbids the EM transitions between two states $|I_i M_i K_i\rangle$ and $|I_f M_f K_f\rangle$ for which the forbiddenness $\nu \equiv |\Delta K| - \lambda$ is greater than zero, where λ is the multipole order and $\Delta K \equiv K_f - K_i$. The degree of hindrance of a K-forbidden transition can be expressed in terms of the "reduced hindrance" $f_\nu \equiv [B(\mathcal{M}\lambda)_{\text{W.u.}}/B(\mathcal{M}\lambda)]^{\frac{1}{\nu}}$, where $B(\mathcal{M}\lambda)_{\text{W.u.}}$ is the Weisskopf single-particle estimate of the EM reduced transition probability. For K-forbidden transitions, f_ν is expected to be $\gg 1$.

Both the EM excitation and decay of high-K states can be greatly hindered by conservation of the K quantum number. Electromagnetic excitation probabilities decrease by many orders of magnitude with increasing multipole order, whereas for Coulomb excitation (EM excitation during nuclear collisions) the probability of multiple-step excitations decreases approximately exponentially with the number of steps, making the EM excitation of high-K states from the ground state unlikely. For this reason, the Coulomb excitation of the 8^- isomer in ^{178}Hf has remained a mystery during the two

*Current address: School of Physics, Peking University, Beijing 100871, People's Republic of China.
†Current address: Department of Physics, Rhodes College, Memphis, Tennessee 38112, USA.

decades since it was first reported by Hamilton *et al.* [8] and since its verification by Xie *et al.* [9] in 1993. The unexpected population of high-K isomers to measurable levels by Coulomb excitation has brought into question the validity or "goodness" of the K quantum number.

Predictions of the hindrance values of K-isomer decays have been made based on a number of mechanisms, and a variety of measurements have suggested that more than one mechanism may need to be considered [2,10–12]. The γ-barrier tunneling model has been successful in reproducing measured hindrances for some nuclei [1,13], but has both overpredicted and underpredicted transition probabilities for others [11,14,15]. Projected shell-model (PSM) calculations have been proposed to treat softness to γ deformation [16,17]. Calculations have been made [18] based on a statistical process of successive rotational alignments, using the tilted-axis cranking (TAC) model [19]. This alternative to γ tunneling has had some success in describing K-isomer decay in ^{178}Hf. Neither the PSM nor the TAC approach has been fully developed at present.

A Coriolis K-mixing calculation for K-forbidden transitions of apparently low hindrance has been demonstrated [20] to recover the "Rusinov rule" [21], $f_\nu \sim 100$, by adjusting the forbiddenness ν for the K admixtures in the isomer state. However, at least one quantitative measurement has shown a high-K isomer to be very pure in K [22]. Allusions to the admixture of high-K components in the wave functions of states in the yrast band have been under consideration for many years [2], and recent measurements reiterate the possibility (e.g., Refs. [12,20]). K-mixing calculations for high-K isomer states, based on density of states considerations, have reproduced some, but not all, of the observed systematics [10].

The Coulomb excitation work of Hamilton [8] and Xie [9] measured only the yield of the $K^\pi = 8^-$ isomer state of ^{178}Hf, showing the overall influence of the K-selection rule in terms of the total isomer excitation cross sections. To find the path through the nuclear states and the EM matrix elements connecting the ground-state band (GSB) to the 8^- isomer band, it is necessary to measure the accompanying excitation of the individual rotational states built on the isomer. The pair of experiments in the present work will be shown to determine the excitation paths of the 8^- isomer as well as the 6^+ and 16^+ isomers in ^{178}Hf. The rate at which the onset of K-selection violations occurs with increasing spin is determined, and this is shown to be consistent with a rotational alignment picture.

This work comprises two separate Coulomb excitation experiments. In the first, a 650-MeV ^{136}Xe beam was incident on a ^{178}Hf target. Projectile and target ions were counted in kinematic coincidence using CHICO [23], Rochester's parallel plate avalanche counter (PPAC), and γ-ray data were collected in Gammasphere [24]. Matrix elements coupling the $K^\pi = 0^+, 2^+, 4^+, 6^+_{\rm isom}(t_{\frac{1}{2}} = 77$ ns), $8^-_{\rm isom}(t_{\frac{1}{2}} = 4$ s), and $16^+_{\rm isom}(t_{\frac{1}{2}} = 31$ yr) bands were fit to prompt and delayed γ-ray yields. Unexpectedly high yields from the $19^+_{K=16} \rightarrow 18^+_{K=16}$ transition in the four-quasiparticle $K^\pi = 16^+$ band were measured to be $\sim 10^{-3}$ of the $8^+_{\rm GSB} \rightarrow 6^+_{\rm GSB}$ transition. In the second experiment, directed at verifying the EM population of the 16^+ isomer, a ^{178}Hf beam was activated into the $16^+_{\rm isom}$ state at five beam energies and trapped in natural tantalum foils. An activation function for the isomer covering 73–86% of the Coulomb barrier $E_{\rm Coul}$ was used to find a set of matrix elements coupling the GSB to the $K = 16$ isomer band.

Sections II–III of this article detail the two experiments and their analyses, including a significantly extended level scheme with a possible extension to the lowest known $K = 0$ band obtained from experiment I. The fit of matrix elements that populate the $K^\pi = 16^+$ isomer band was accomplished through a combined analysis of the first and second experiments, described in Sec. IV. Section V A covers the measurements of the EM properties of the nucleus, including measured quadrupole moments, the gyromagnetic ratios of the $K^\pi = 6^+$ isomer band, and the band mixing between the two 8^- bands at 1147 keV and 1479 keV. Conclusions regarding the goodness of the K-quantum number constitute the majority of Sec. V.

II. EXPERIMENT

A. ^{178}Hf(^{136}Xe,^{136}Xe)^{178}Hf coulomb excitation

To resolve γ rays in complex spectra, the γ-ray energies must be measured to an accuracy of the order of 1%. To achieve this in a thin-target experiment, where the γ rays are emitted in flight, the detector system must support event-by-event correction of the Doppler-shifted γ-ray energies. This was accomplished in the first of the two experiments described herein by utilizing 100 of 110 elements of the 4π Gammasphere array and CHICO. Gammasphere was fitted with 0.002-in.-thick Ta and 0.010-in.-thick Cu absorbers over the germanium faces to attenuate low energy ($\lesssim$100 keV) photons and prevent the flooding of the detector with atomic x rays, resulting in a p-p-γ (two particles and at least one γ ray) trigger rate of 4 kHz. The total photopeak detection efficiency for a γ ray in Gammasphere is 9% at 1.3 MeV, so that γ-ray triples (triple-coincidence γ-ray events) can be collected with good statistics. CHICO consists of 20 isobutane-filled PPACs, which are capable of detecting light and heavy ions, including α particles, and identifying the scattered particles by kinematic coincidence with a typical mass resolution of 5%, an angular coverage of $12^\circ < \theta < 85^\circ$ and $95^\circ < \theta < 168^\circ$ in the polar angle, and an acceptance of 2.8π sr or 69% of the sphere. The ATLAS superconducting linac at Argonne National Laboratory provided a 650-MeV ^{136}Xe beam for a total of $\approx$76 hours, incident on a 0.51 mg/cm^2, 89% enriched ^{178}Hf target supported by a 0.035 mg/cm^2 carbon foil. A 1 μs sweeper interrupted the beam, allowing the detection of delayed γ rays from isomer decays with 10 ns $\lesssim t_{\frac{1}{2}} \lesssim 1$ μs. The target comprised six species in the following molar fractions: <0.05% ^{174}Hf, 0.52(5)% ^{176}Hf, 4.36(5)% ^{177}Hf, 89.14(10)% ^{178}Hf, 2.90(5)% ^{179}Hf, 3.07(5)% ^{180}Hf.

Approximately 5×10^8 usable p-p-γ events were recorded (two particles coincident detected by CHICO plus at least one γ ray detected by Gammasphere). Scaled-down singles (p-p events with no γ ray required) were not utilized, which necessitated the normalization of all γ-ray yields to the strong $8^+_{\rm GSB} \rightarrow 6^+_{\rm GSB}$ transition. Because the normalization was not absolute in terms of the cross section, these are referred to below as "relative yields." The γ-ray detection efficiency was

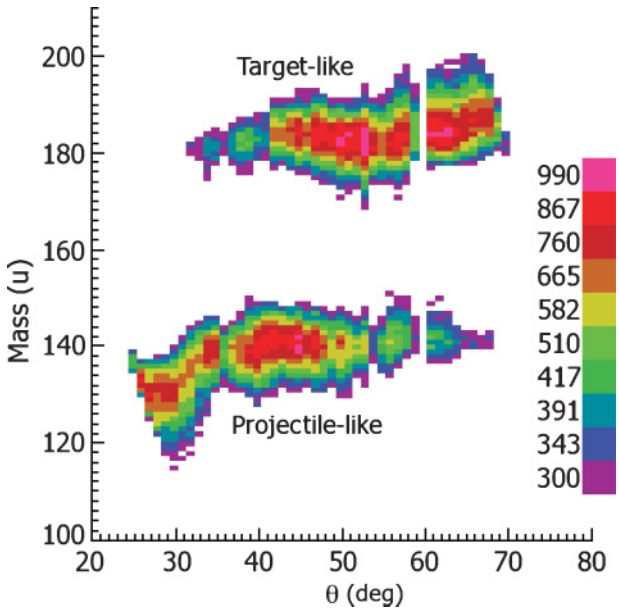

FIG. 1. (Color online) A two-dimensional histogram of mass m versus θ with a lower limit at 300 counts for clarity.

measured as a function of E_γ using data from the GSB γ-ray cascades of four isotopes: ^{238}U, ^{152}Eu, ^{170}Er, and ^{178}Hf. The ^{238}U and ^{170}Er efficiency data were obtained from a 1358-MeV ^{238}U on ^{170}Er experiment [25,26] that ran immediately after the present Hf measurement, and the ^{152}Eu data were obtained from a $\approx$5-μCi source calibration run.

The time-of-flight difference Δt and the angle θ between the scattered beam and recoiling target ions was measured by CHICO and transformed into mass m vs. θ (Fig. 1), where the two kinematic solutions are clearly separated. Event-by-event Doppler correction resulted in a 0.5% ΔE_γ resolution, sufficient to measure γ-ray yields to the 10^{-4} level relative to the $8^+_{\rm GSB} \rightarrow 6^+_{\rm GSB}$ yield.

Figure 2 shows the level scheme derived from this experiment. The p-p-γ singles spectra were effective in measuring the $\gtrsim$1% yields of strongly populated states in the GSB and the lower levels of the γ band. Prompt-prompt γ-γ matrices were effective in measuring the γ-band decays to the GSB. Prompt-delayed γ-γ matrices were constructed from the data in 9° intervals in the projectile (Xe) scattering angle $\theta^{\rm lab}_{\rm scat}$. The prompt-delayed matrices provided a high selectivity for measuring the yields of the $K = 6^+$ isomer band, where the $t_{\frac{1}{2}} = 77$ ns half-life permitted correlations between the prompt intraband transitions and the isomer decays. Symmetric cubes of threefold γ-ray events were analyzed using the RADWARE package [27] to measure the yields of the remaining bands, populated below the 10^{-2} probability level.

B. $K^\pi = 16^+$ isomer activation experiment

The Hf^{178}(^{136}Xe,^{136}Xe)Hf^{178} Coulomb excitation experiment measured a remarkably high $19^+ \rightarrow 18^+$ yield (Fig. 2) in the $K^\pi = 16^+$ isomer band. This second experiment was devised to measure the Coulomb excitation of the 16^+ isomer by its activity as a function of collision energy to confirm that the 16^+ band population followed Coulomb excitation predictions and to extract a set of $\langle I_{K=16^+} \| E2 \| I_{\rm GSB} \rangle$ matrix elements. A stack of five 1 mg/cm^2 natural Ta targets was irradiated by a $\approx$10-pnA ^{178}Hf $^{24+}$ beam from ATLAS, providing an excitation function over a centroid bombarding energy range of 73% (target 5) to 86% (target 1) $E_{\rm Coul}$. The incident beam energy of 858 MeV was chosen to give $E_{\rm beam} \leqslant 80\%\ E_{\rm Coul}$ for the third, fourth, and fifth targets, so that nuclear effects would be small or insignificant in all five Ta targets [28–30].

The targets were arranged normal to the beam, separated by 0.59-cm-long, 1.0-cm-diameter hollow cylindrical 42-mg/cm^2 tantalum "catchers" to collect scattered Hf ions over $40^\circ \leqslant \theta^{\rm lab}_{\rm scat} \leqslant 90^\circ$, so that $\ll$1% of the nuclei in the 16^+ state were lost or embedded in downstream targets. The target stack was biased at +4 kV to prevent a scattered electron current in the Faraday cup. A 1 mg/cm^2 Ta scattering foil was used to scatter beam and target particles into a silicon monitor detector mounted at $\theta^{\rm lab}_{\rm scat} = 45^\circ$. The rate was reduced to $\approx$30 Hz using a collimator mounted on the face of the silicon detector. Faraday cup and silicon data provided an absolute measurement of the total beam dose of 1.7(2) particle-mC (particle-milli-Coulombs) to normalize the absolute activation cross sections. A germanium detector monitored the prompt online γ rays emitted by Hf nuclei stopped in the Faraday cup to measure target ablation as a function of time and to monitor the beam species. The 25-cm-long, 3-cm-diameter Faraday cup was mounted with its downstream end 43 cm from the center of the target chamber.

Deviations of the beam position on target and small-angle scattering did not introduce significant errors into the activation rate measurement. Calculations using SMSCAT [31] showed that $\sim$10% of the Hf ions scattered on the first target would be displaced by $\leqslant$0.2 mm at the end of the target stack, and the errors introduced by electronic scattering would be small compared to other effects, such as target ablation.

The activities in the targets and catcher foils were counted 5 months after the activation at Yale University's Wright Nuclear Structure Laboratory. Offline counting of the isomer decays via the cascade shown in Fig. 3 provided the cross section measurements. The targets were positioned between two four-crystal "clover" Ge detectors, which were arranged with their front faces 1 mm apart and shielded by several inches of lead on all four sides. The detectors were composed of four approximately cylindrical crystals that were read individually. A target foil and its catcher were positioned between the clovers, equidistant from all eight crystals and counted for times ranging from 16.5 to 237 h (Table I). In every case, the target foil and its catcher foil (unrolled and flattened from its original cylindrical shape) were counted simultaneously. (Target 2, excited at 83% $E_{\rm Coul}$, was not measured.) The foil and catcher pairs were positioned overlapping at the center of the detector pair so that they resembled point sources as closely as possible, simplifying the analysis. Both the foil and the catcher were thin enough to cause negligible γ-ray attenuation. Relative γ-ray efficiency data were taken using a ^{152}Eu source.

The quiet background and unexpectedly high count rate in the clover detectors showed remarkably prominent ^{178}Hf

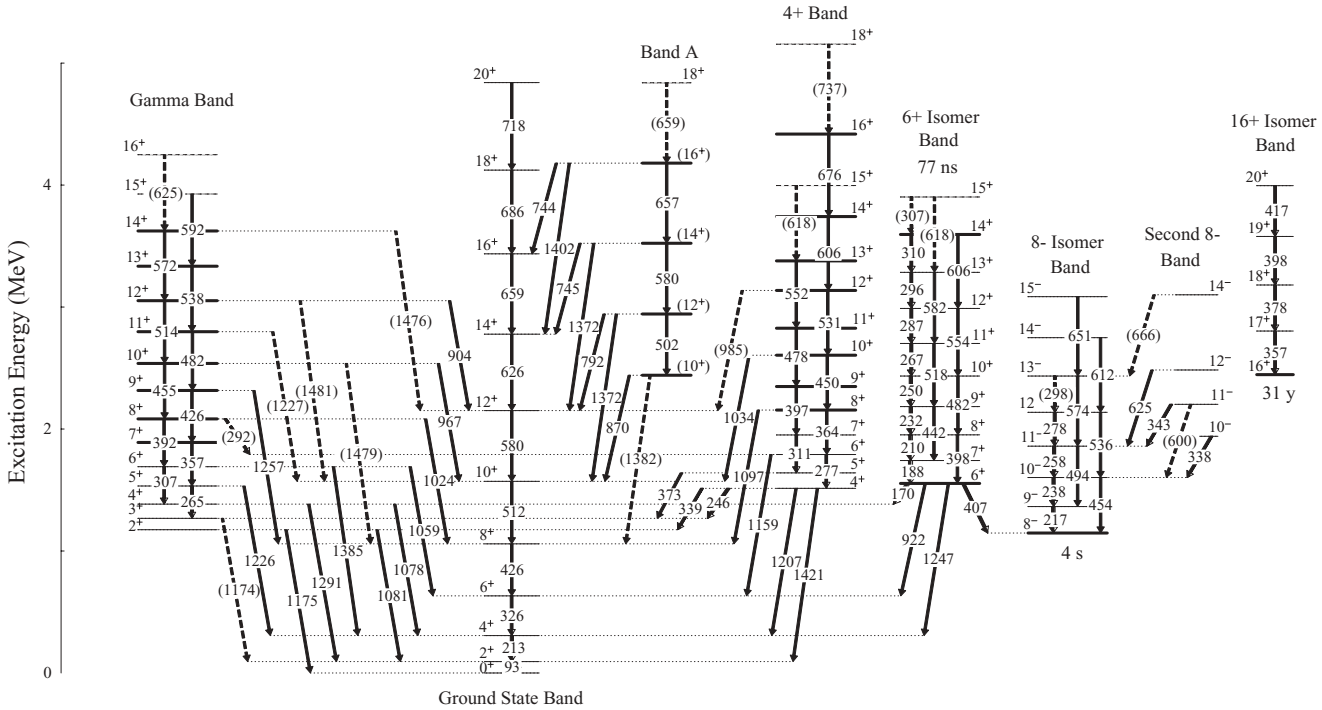

FIG. 2. Master level scheme showing all of the levels observed in the ^{178}Hf(^{136}Xe,^{136}Xe)^{178}Hf experiment. New levels and isomer states are shown as bold horizontal lines. Dashed horizontal lines represent tentatively placed states.

peaks due to the isomer activity (Fig. 4). The GSB peaks are well above background, as well as some $K = 8^-$ in-band transitions and the 88-keV decay of the 8^- isomer to the $8^+_{K=0}$ state. Ideally, the activity could be measured by counting either the 8^- band cascades or the GSB cascades, but the latter provided more accurate results because no knowledge of branching ratios was required. The peak-to-background ratio of the single-γ spectrum was not high enough (4% for target 5) to accurately measure the activation of the lower energy targets. Better statistics were obtained from the $n > 1$-fold (twofold and higher) matrix by gating on a GSB transition and counting the coincident γ rays in the GSB (Fig. 5).

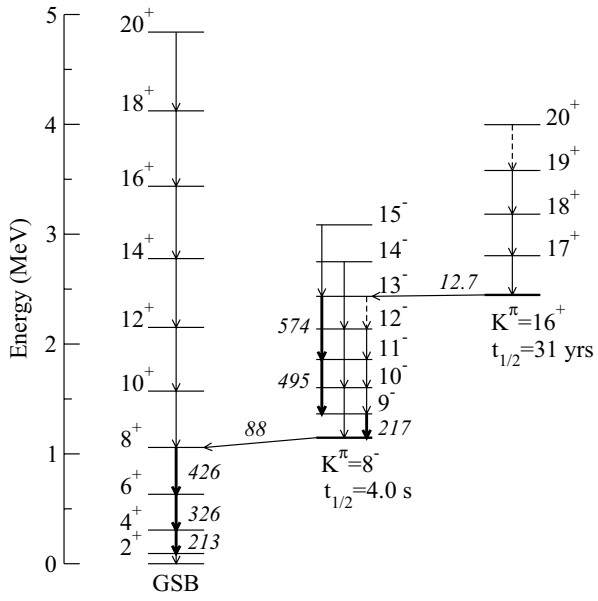

FIG. 3. A partial level diagram for ^{178}Hf built from the data of the Hf(Xe, Xe)Hf and Ta(Hf,Hf)Ta experiments. The known 12.7-keV transition was not observed. The strongest decay cascade (bold arrows) is known from branching ratios. The $\Delta I = 1$ branch from the 13^- level accounts for only ~10% of the total decay width.

To correct for the target ablation over time and to measure the total integrated dose for the entire second experiment, the Si detector was used to calibrate the Faraday cup early in the experiment, and the integrated current from the Faraday cup was used to measure the dose in the remaining runs. The absolute cross sections for excitation to the $K = 16^+$ isomer state were calculated from the total beam dose and the initial average areal density of the scattering target, $\rho_A = 1.0(1)$ mg/cm^2.

TABLE I. Count times and raw count rates of GSB transitions (uncorrected for counting efficiency) for each target. Count rates are from γ-ray singles.

Target	Counting time (h)	Single-γ count rates (h^{-1})		
		$6^+ \rightarrow 4^+$	$8^+ \rightarrow 6^+$	$10^+ \rightarrow 8^+$
1	16.5	195(12)	173(10)	123(9)
2[a]	–	–	–	–
3	17.5	67(9)	80(6)	73(7)
4	105.6	29(14)	24(2)	17(2)
5	237		6.9(16)	11(1)

[a]Target 2 was not counted.

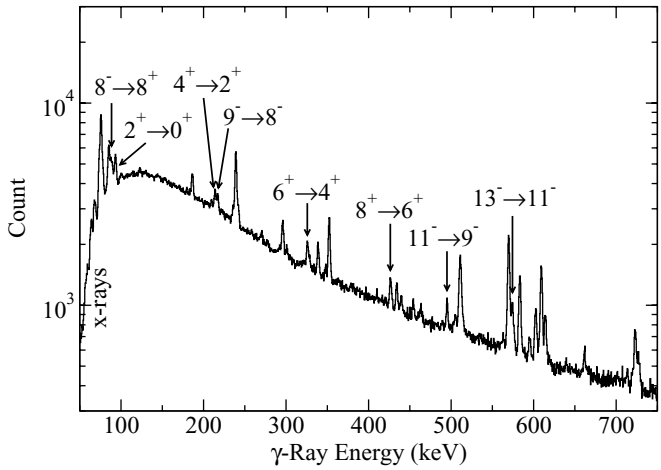

FIG. 4. A raw γ-ray singles spectrum from the ^{178}Hf beam activation experiment. The data from the activity of target 1 after 16 h of postactivation data collection are presented.

III. ANALYSIS

A. Levels and bands

The power of the combination of Gammasphere and CHICO is evident not only from the ability to measure yields to the 10^{-4} level in the ^{178}Hf target nucleus but also from the data gleaned from isotopic impurities at the 0.5–4% level, using p-p-γ-γ-γ triples data. Data from γ-ray singles (p-p-γ) and gated doubles and triples were used to extend several previously known rotational bands in ^{178}Hf [32–34] as shown in Fig. 2 and described below. In addition, intermediate states tentatively connected to a previously known $K^\pi = 0^+$ band [35–38] were discovered.

1. The GSB and the γ band

The $20^+_{\rm GSB}$ level in ^{178}Hf found by Mullins *et al.* [32] was confirmed, but a 22^+ level could not be found. The γ band,

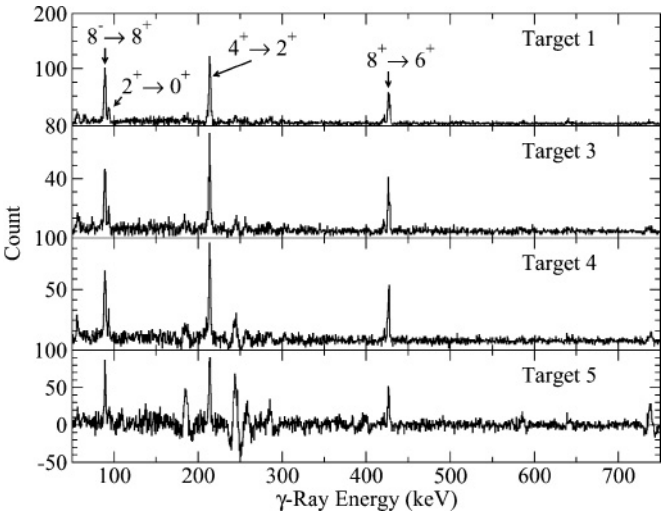

FIG. 5. Four background-subtracted γ-ray doubles spectra gated on the 326 keV $6^+_{\rm GSB} \rightarrow 4^+_{\rm GSB}$ transition of ^{178}Hf. Transitions from the 8^- isomer decay cascade are indicated by arrows.

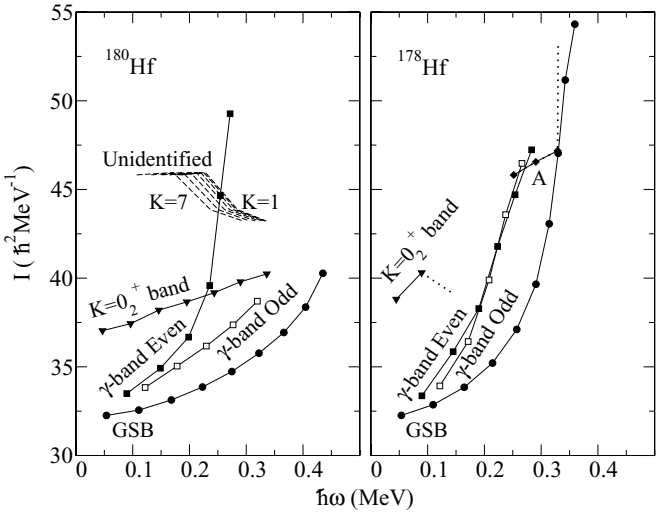

FIG. 6. Moments of inertia of several bands in ^{180}Hf (left) [39,40] and ^{178}Hf (right). Tentative levels are shown by dotted lines. The lowest frequency point in each curve corresponds to $I = K + 2$, except for band A, which begins with $I = 12$(tentative). Band 7 of [39] is shown as a set of dashed lines for a range of possible K values.

with a band head at 1175 keV, previously known up to the 6^+ level, was extended to the 14^+ level with tentative 15^+ and 16^+ states. The γ band's even and odd signatures have nearly equal moments of inertia and do not diverge up to spin $16\hbar$, in contrast with the strong signature splitting and diverging moments seen in ^{180}Hf [39,40] (Fig. 6). This indicates a major change in the interaction between the GSB and the γ band on the addition of two $i_{13/2}$ neutrons.

2. A possible extension to the $K^\pi = 0^+_2$ band

Four intermediate levels and a tentative fifth level in the unidentified band "A" (Fig. 2) were observed feeding into the GSB, suggesting a small K value. The spacing of the observed states, as well as the decay pattern into the GSB, indicate that the observed intraband decays of band A are likely $\Delta I = 2$ transitions. The relative yields, normalized to the $8^+_{\rm GSB} \rightarrow 6^+_{\rm GSB}$ transition for a scattering angle range of $52^\circ \leqslant \theta^{\rm lab}_{\rm scat} \leqslant 78^\circ$ were measured using the γ-ray triples (Fig. 7). The branching ratios needed to correct for effects due to coincidence gating were not measurable, but one intraband yield and three lower limits were found. From the decay pattern and the level spacing, possible spin-parity assignments for the lowest observed state are 10^+, 9^-, and 8^+. Odd parity is assumed for spin 9, because only one signature of the band is seen, more likely the natural parity states. Dominant $\Delta I = -2$ γ decays from lower states to the GSB were not observed and may have been obscured by the large Doppler-broadened 1.3 MeV ^{136}Xe $2^+ \rightarrow 0^+$ transition.

An exhaustive search for the complete set of lower levels for the band was undertaken using the present γ-ray data and the known levels and bands in ^{178}Hf (e.g., Refs. [32,34,37,41,42]) and testing all possible values of K and spin-parity. The measured moments of inertia of Fig. 6 and comparison to the

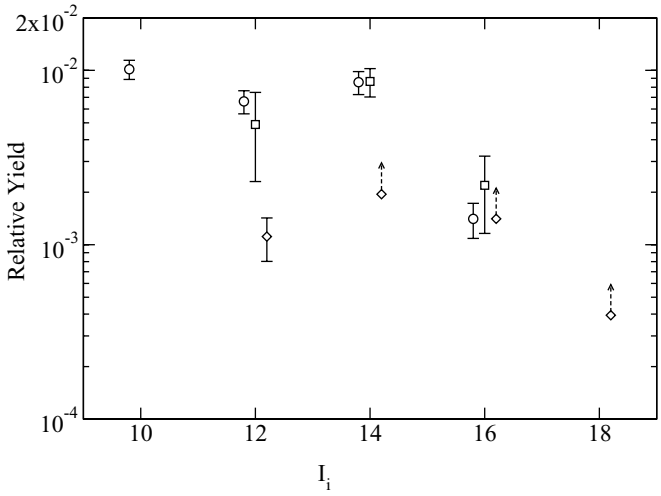

FIG. 7. Yield vs. spin for decays from band A, normalized to the $8^+_{\rm GSB} \rightarrow 6^+_{\rm GSB}$ transition for $52^\circ \leqslant \theta^{\rm lab}_{\rm scat} \leqslant 78^\circ$. Yields are shown for $\Delta I = 0$ (circles) and $\Delta I = -2$ (squares) transitions to the GSB and for intraband $\Delta I = -2$ transitions (diamonds) from the initial state of spin I_i in band A.

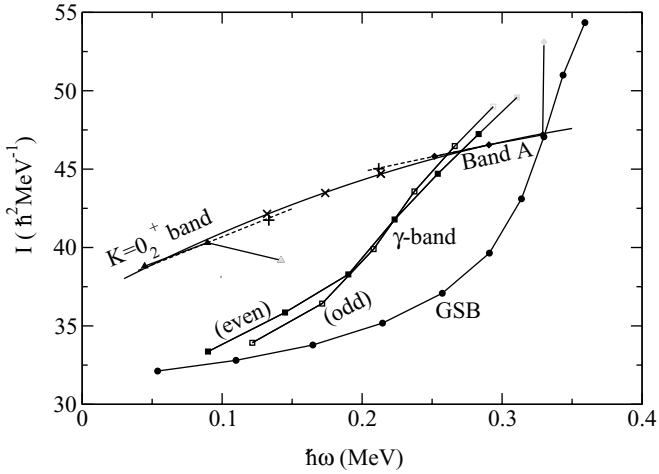

FIG. 8. Measured moments of inertia for levels in the lowest excited $K^\pi = 0^+$ band ("$K^\pi = 0^+_2$") and band A, connected by a quadratic fit to the firm levels, suggesting interpolated moments of the 6^+, 8^+, and 10^+ states (x's). Linear fits to two levels each in band A and in the $K^\pi = 0^+_2$ band suggest extrapolated moments of the 6^+ and 10^+ levels (+'s). The highest spin members of the γ band, the known $K^\pi = 0^+_2$ band and band A are tentatively placed (see text).

^{180}Hf Coulomb excitation data of Ngijoi-Yogo *et al.* [39,40] suggest that band A could be the continuation of the $K^\pi = 0^+_2$ band (Fig. 6). The $I^\pi = 0^+_2$ state in ^{178}Hf was characterized as a β vibration by Nielsen *et al.* [35,36], but the most recent measurement of $0.3 < B(E2; 2^+_2 \rightarrow 0^+_{\rm GSB}) < 1.5$ W.u., a strength typical of single-particle transitions, shows that the vibrational character of the $I^\pi = 0^+_2$ state is an open question [38]. Nonetheless, the similarity between the moments of inertia of band A and the $K^\pi = 0^+_2$ band of Refs. [39,40] supports the $K = 0$ identification of band A.

Because the moment of inertia for a particular level is very sensitive to the intraband decay energies, an accurate interpolation of the missing levels' moments would give a precise indication of the expected intermediate γ-ray energies if band A is a continuation of the $K^\pi = 0^+_2$ band. Figure 8 shows a parabolic fit to the moments of the 2^+ and 4^+ levels of the $K^\pi = 0^+_2$ band and the 12^+–16^+ levels of band A, as well as linear extrapolations from the $K^\pi = 0^+_2$ and A bands. None of the sets of interpolated or extrapolated γ-ray energies was found in the data, presumably because the interband decay branches dominate the decay. No other coincidental sets of γ rays were found which gave the correct sum energy.

The tentative identification of the 6^+ level of the $K^\pi = 0^+_2$ band at 1731 keV in previous work [41] was based on a multiply placed transition, which some authors have suggested feeds the $4^+_{K=0_2}$ level [34]. If the 6^+ level energy is correct, and band A is the $K^\pi = 0^+_2$ band, this implies that the moment of inertia of the band oscillates by $\approx \pm 5\hbar^2$/MeV between the 6^+ and 10^+ levels, to satisfy the correct γ-ray sum energy. This seems unlikely, considering the measured moments shown in Fig. 8.

If the $K^\pi = 0^+_2$ bands in ^{178,180}Hf share the same structure, then relative yields of the suspected $K^\pi = 0^+_2$ bands in both nuclei should be similar and less than the relative yields of the γ bands. At the 10^+ levels, the total relative yield $r_{^{178}\rm Hf} \equiv Y_{\rm bandA}/Y_{\gamma-\rm band}$ is 0.7(2). The relative yield of the $10^+_{K=0_2}$ state in the Coulomb excitation of ^{180}Hf is $r_{^{180}\rm Hf,^{136}Xe} = 0.33(3)$, calculated from the data of [39,40] and corrected for the greater population of the 10^+_γ level relative to the GSB. Constraints on the energy sum and a smoothly varying moment of inertia suggest that the $6^+_{K=0_2}$ level currently assigned at 1731 keV [41] will be found closer to 1700 keV. An increase in the $K^\pi = 0^+_2$ band's moment of inertia at spin $\gtrapprox 6\hbar$ is predicted from the present data.

3. High-K bands

a. The 4^+ band at 1514 keV. The tentative 7^+ level [33] in the previously known 4^+ band at 1514 keV was confirmed, and the band was extended from spin 7^+ to spin 16^+ with tentative 15^+ and 18^+ levels.

b. The 6^+ isomer band at 1554 keV. A 14^+ level was added to the 6^+ isomer band, along with a tentative 15^+ level. The moment of inertia exhibits an up-bend above spin $12\hbar$, which is not seen in the other isomer bands.

c. The 8^- bands at 1174 keV and 1479 keV. The 8^-_1 (isomer) and 8^-_2 (1479 keV) bands were observed up to spin 15^-, but new levels were not found.

d. The 16^+ band at 2446 keV. The $K^\pi = 16^+$ levels up to 20^+ were seen in the prompt triple-γ data of the Hf(Xe, Xe)Hf experiment. The intraband γ-decay yields were measured for the $19^+ \rightarrow 18^+$ transition, but the yield of the $20^+ \rightarrow 19^+$ transition was too small to measure in the $9^\circ \theta^{\rm lab}_{\rm scat}$ intervals.

4. Other isotopes

The high sensitivity of the CHICO+Gammasphere combination permitted observation of the GSB states (Fig. 9) up to $\approx 20\hbar$ in all but the least abundant isotope, ^{174}Hf. The

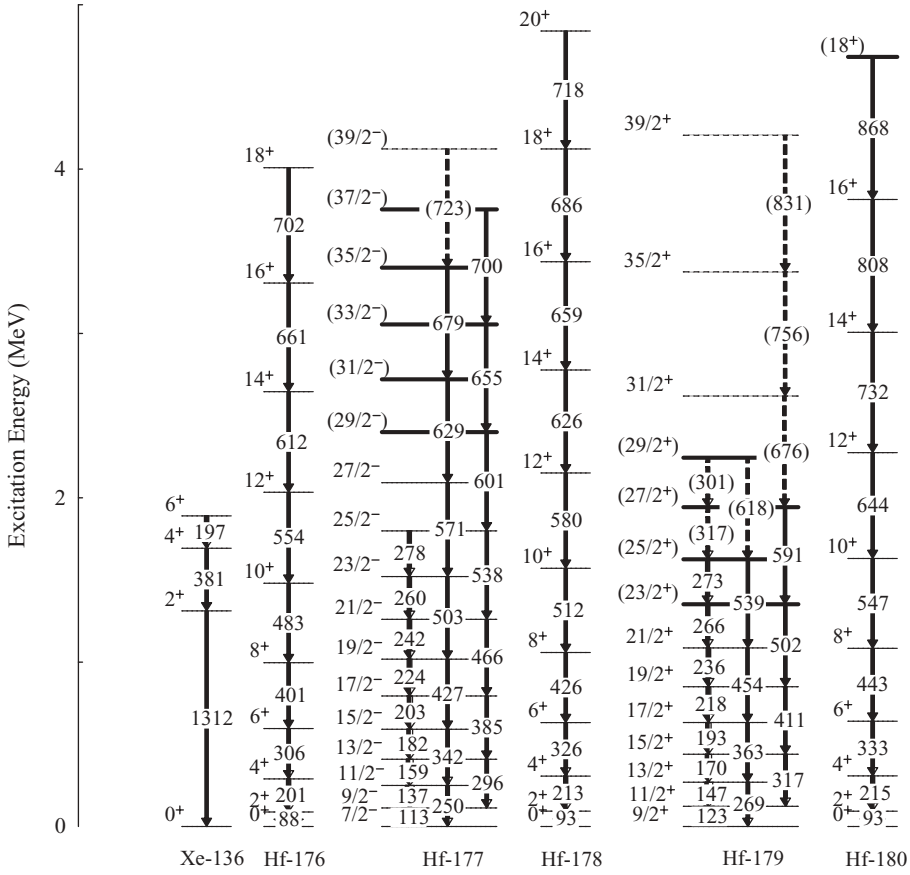

FIG. 9. Isotopes observed in the γ-ray data, showing the ground-state bands of the Hf isotopes in the target foil and the ^{136}Xe $\pi(g\frac{7}{2})^2$ multiplet that was excited in the beam particles. New levels are given as bold horizontal lines. Dashed horizontal lines represent tentatively placed states.

GS band of ^{177}Hf was observed to the previously known $39/2^-$ level [43], and the GSB of ^{179}Hf was extended from the $21/2^+$ level [43] to a tentative $39/2^+$ level (Fig. 9). Trace contaminants of ^{176}Hf made the GSB visible up to the 18^+ state. The GSB of ^{180}Hf was extended from spin 12^+ to spin 18^+, using data from the 3% ^{180}Hf impurity. Ngijoi-Yogo [39,40] independently placed the 18^+ level in an inelastic-scattering experiment that used a 750 MeV ^{136}Xe beam on a ^{180}Hf target.

B. Yield measurements

In the p-p-γ singles spectrum, the yields of the GSB up to the 14^+ level were recorded in 2° intervals over $20^\circ \leqslant \theta^{\rm lab}_{\rm scat} \leqslant 80^\circ$. The yields ($\gtrsim 10^{-4}$ relative to the GSB) of most bands were obtained from the γ-ray triples (e.g., Fig. 10) binned in 9° intervals with the notable exception of the 6^+ isomer band intraband yields, which were selected by a gate on the delayed (50 ns $< t <$ 500 ns) isomer decays to the $6^+_{\rm GSB}$ state in a prompt-delayed matrix (Fig. 11). The yields obtained from the prompt-delayed data were normalized to the relative yields from prompt γ-ray data using the $9^+_{K=6} \rightarrow 8^+_{K=6}$ transition.

In the Hf(Xe, Xe)Hf experiment, the γ-ray yields were normalized to the $8^+_{\rm GSB} \rightarrow 6^+_{\rm GSB}$ transition, which is the lowest-spin transition having good statistics in the gated triples data. Relative yields were corrected for γ-ray efficiency and for the branching ratios and internal conversion of the gate transitions. In the strongly populated levels of the γ band and the GSB, the uncertainty in the γ-ray detection efficiency introduced the majority of the error, generally ≈5% error for each γ ray gated or measured.

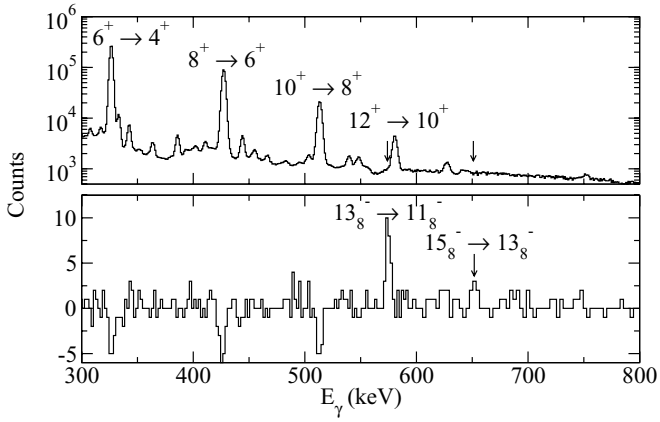

FIG. 10. Typical γ-ray energy spectra for a scattering angle range $52^\circ < \theta^{\rm lab}_{\rm scat} < 61^\circ$. The upper histogram is a p-p-γ singles spectrum with the ^{178}Hf GSB transitions labeled. Arrows indicate the positions of the $13^-_{K=8} \rightarrow 11^-_{K=8}$ and $15^-_{K=8} \rightarrow 13^-_{K=8}$ transitions. Most of the smaller peaks are GSB transitions from other isotopes. The lower histogram is the resultant background-subtracted spectrum from a gate on the $9^- \rightarrow 8^-$ and $11^- \rightarrow 9^-$ transitions in the 8^- isomer band. The small oversubtraction of the background is due to coincidences between strong peaks and the background.

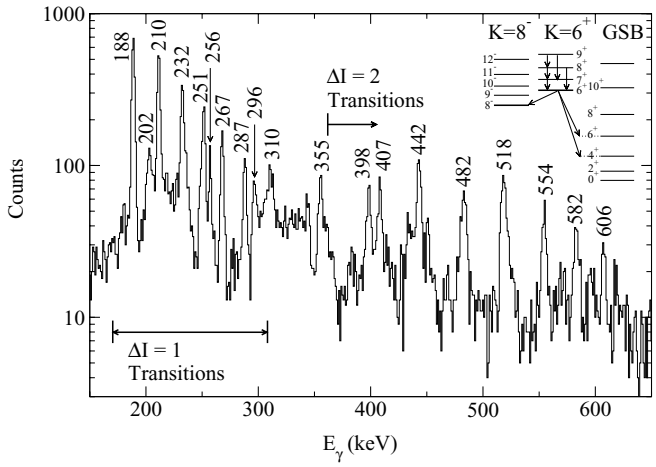

FIG. 11. A background-subtracted prompt resultant γ-ray spectrum from a gate on the delayed $6^+_{\rm isom} \rightarrow 6^+_{\rm GSB}$ transition. The $\Delta I = 1$ and $\Delta I = 2$ intraband transitions are labeled by their energies in keV. Several unidentified peaks, such as the 202- and 296-keV peaks appear to be the result of random coincidences between strong GSB yields and delayed $6^+_{\rm isom}$ decays from different events to which the Doppler-shift correction was inappropriately applied. (The broadened 213- and 326-keV GSB transitions can be seen.)

The prompt-delayed data also provided a precise measurement of the branching ratios of the 6^+ isomer decays. The highly converted 40-keV decay branch to the $K^\pi = 4^+$ band head [44], was measured indirectly in this work by the intensities of the secondary decays of the 4^+ band head (Table II). The previously unmeasured strength of this branch accounts for 19(1)% of the 6^+ isomer decay width, including conversion, and is essential in correctly determining the Coulomb excitation paths to the 6^+ isomer band. The branching ratios of Hague *et al.* [41] are compared with the present measurements in Table II. The agreement is better when Hague's values are adjusted for the previously unmeasured strength of the $6^+_{K=6} \overset{E2}{\rightarrow} 4^+_{K=4}$ branch.

1. The $K^\pi = 8^-$ bands

Some 8^- isomer band yields were obtained from prompt triples, although only three clean gates ($12^- \rightarrow 11^-$, $11^- \rightarrow 10^-$, and $11^- \rightarrow 9^-$) could be distinguished from GSB transitions in the odd-A isotopes of the target. Yields could be extracted down to approximately the 10^{-4} level. Five interband feeding transitions from the upper 8^-_2 band were observed, just above the lower limit of observation, by gating in the 8^-_1 isomer band. Intraband branches in the upper 8^-_2 band were not observed.

2. The $K^\pi = 16^+$ band

The 16^+ isomer band, previously known up to a tentative 23^+ state [32], was unexpectedly populated at the $\sim 10^{-4}$ level up to spin 20^+ in the Hf(Xe, Xe)Hf experiment. The low intensity and the 31-yr half-life required prompt triples gating, so the only measurable yields in 9° $\theta^{\rm lab}_{\rm scat}$ intervals were observed for the $19^+ \rightarrow 18^+$ transition. More information was derived from the ^{178}Hf activation experiment.

In determining the activation cross sections for the $K^\pi = 16^+, t_{\frac{1}{2}} = 31$ yr isomer, the measured doubles (γ-γ) rates of the 326- and 426-keV transitions are proportional to the product $\kappa \epsilon P$ for each γ ray, where κ is the correction for internal conversion, ϵ is the absolute detection efficiency, and P is the peak-to-total ratio, calculated from the measured ratio of γ doubles to γ singles. It was found that $P = 0.74(7)$ and 0.64(6) for the 426- and 326-keV transitions, respectively, measured using target 1. It should be noted that the γ-γ doubles and γ singles activities are not independent for target 1, because the singles rate was used to measure the peak-to-total ratio. Summing (capture of two or more γ rays in the same Ge crystal) and detection probabilities were both treated using calculated angular correlation functions. The second-order and fourth-order angular correlation terms gave $\approx$10% and $\approx$1% contributions, respectively, and the total angular correlation corrections were $<$10% in all cases. Corrections to the γ-ray efficiency were made for the oblique trajectory through the Ge crystals. The measured activities of the targets are given in Table III for the two single-γ transitions measured and the $\gamma\gamma$ measurement using the 326- and 426-keV transitions.

The cross sections provided in Table III are calculated for the average target thickness during the ablation of the target material. This introduces a $\approx$20% error in σ_{16^+}, calculated from the change in the calculated cross section as the integration limits in projectile energy change over time.

TABLE II. The measured reduced transition strengths $B(\mathcal{M}\lambda; 6^+_{K=6} \rightarrow I^\pi_f, K)$ for the decay branches of the 6^+ isomer, compared with values tabulated in Ref. [51] from the data of Hague *et al.* [41]. The Weisskopf unit is taken in the downward direction. The adjusted values are explained in the text.

Decay branch	E_γ (keV)	$\alpha_{\rm IC}$	Reduced transition probability (W.u.)		
			This work	Hague	Hague, adj.
$6^+_{K=6} \overset{E2}{\rightarrow} 6^+_{\rm GSB}$	922	0.00498	$8.6(6) \times 10^{-5}$	$1.10(7) \times 10^{-4}$	8.94×10^{-5}
$6^+_6 \overset{E2}{\rightarrow} 4^+_{\rm GSB}$	1247	0.00268	$1.16(9) \times 10^{-5}$	$1.25(6) \times 10^{-5}$	1.02×10^{-5}
$6^+_{K=6} \overset{M2}{\rightarrow} 8^-_{K=8}$	407	0.291	0.020(3)	0.0269(15)	0.0219
$6^+_{K=6} \overset{E2}{\rightarrow} 4^+_{K=4}$	40	216.0	1.03(7)	–	–
$6^+_{K=6} \overset{E2}{\rightarrow} 4^+_{K=2}$	169	0.516	0.018(3)	0.0375(21)	0.0305

TABLE III. Summary of measured activities of the four measured targets. The cross sections σ_{16^+} are calculated from the values D.

E_{beam} (% barrier)	Count time (h)	γ Singles rate (h^{-1})		Doubles $D(h^{-1})$	σ_{16^+} (mb)
		S^{326}	S^{426}		
86 (Targ. 1)	16.5	173.(10)	123.(9)	19.9(14)	11(3)
80 (Targ. 3)	17.5	80.(6)	73.(7)	10.6(10)	6(2)
76 (Targ. 4)	105.6	24.(2)	17.3(15)	2.5(2)	1.4(4)
73 (Targ. 5)	237	6.9(16)	10.9(14)	1.04(9)	0.6(2)

3. *The $K^\pi = 14^-$ band*

The $K^\pi = 14^-$ intraband γ decays were not visible in the data sets, but an upper limit of population strength was set at 50% of the 16^+ band population for the 16^- level, based on a tentative peak in the gated doubles spectra of the Hf(Xe, Xe)Hf experiment. The 1-μs time window for γ-ray collection did not permit observation of the 14^- ($t_{1/2} = 68$ μs) isomer decays.

C. Fit of matrix elements: The $K^\pi = 0^+, 2^+, 4^+$ and 8^- bands

The effectiveness of a particular excitation path between two bands was evaluated using the results of a χ^2 minimization of the calculated γ-ray yields with the coupled-channel semiclassical Coulomb excitation code GOSIA [45]. A pathway was either eliminated as a possibility or confirmed, in which case the intrinsic matrix element was measured as a single parameter connecting the two bands. An excitation path was eliminated if it could not reproduce a significant fraction of the measured yields using reasonable reduced transition probabilities for the particular multipolarity and the change in single-particle structure. In cases where multiple excitation paths were discovered, the relative importance of each can be evaluated by its contribution to the calculated yields at the χ^2 minimum. The Alaga rule was found to reproduce K-allowed transitions well, whereas population by K-forbidden transitions was described well by the spin-dependent mixing (SDM) model (Equation 4-95 in Ref. [7]) in several cases.

For the strongly coupled $K^\pi = 0^+$, 2^+, and 4^+ bands, an iterative fit process was employed to deduce the reduced matrix elements. The quadrupole moment of the most strongly populated band, the GSB, was adjusted first. After finding the matrix elements which gave the minimum value of χ^2, the band with the next highest population, the γ-band, was added to the system along with its measured γ-ray yields. This procedure was repeated, fitting all of the adjustable parameters (quadrupole moments and interband $E2$ and $M1$ matrix elements) at each step. The GSB, the γ band and the 4^+ band were strongly coupled, so that their matrix elements could not be fit independently without the iterative technique. The $K > 4$ bands were treated as small perturbations without any loss of accuracy in the reproduced yields. Final adjustments of each measured matrix element were made by measuring the correlated errors using the criterion $\chi^2(\bar{x} \pm \sigma) = \chi^2(\bar{x}) + 1$, where $\bar{x}$ is the best value at χ^2_{min} [46] (Table IV). For the least-squares fit at unsafe scattering angles beyond $\theta^{\text{lab}}_{\text{scat}} = 52^\circ$, the weight of the data was reduced to $\frac{1}{2}$ ($\frac{1}{4}$, in terms of χ^2) relative to the data from the safe region, so that nuclear interference effects in the data would not greatly influence the purely electromagnetic analysis.

D. Fit of matrix elements: The $K^\pi = 16^+$ band

Because the first experiment showed that the excitation function of the GSB levels can be described accurately assuming a rigid rotor, the 16^+ band's excitation function can in principle be used to extract a large subset of the $\langle I_{K=16} \| E2 \| I_{\text{GSB}} \rangle$ matrix elements. As the beam energy in the target is increased, higher GSB levels become populated with sufficient strength to contribute to the 16^+ isomer activation, and matrix elements coupling higher-spin levels become important. Ideally, one matrix element for each GSB level would be far more effective than the others, either because of the change ΔI in spin or because of the E^5 factor in the γ decay width in cases where feeding dominates.

The 16^+ isomer activity data and the prompt $19^+_{K=16}$ γ-ray yields of the first experiment (Fig. 12) were combined in an effort to find a single set of matrix elements that would reproduce the data of both experiments. An unsuccessful attempt was made to reduce the number of fit parameters using the SDM model, which was found to fail for this high-K band. Ultimately, the GSB$\rightarrow$ $K^\pi = 16^+$ matrix elements were adjusted individually to reproduce the data, observing the

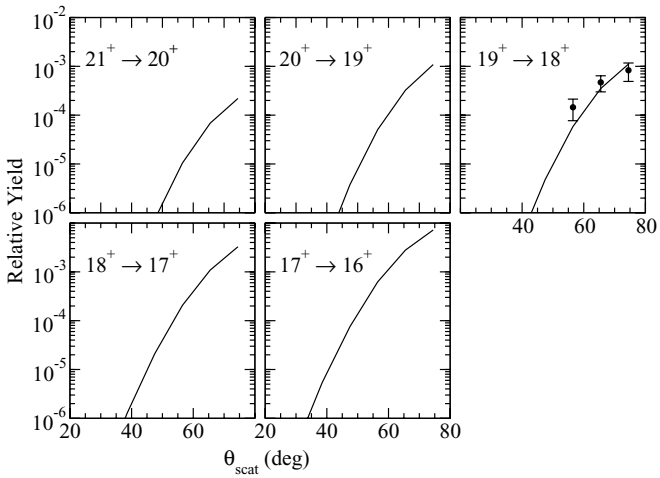

FIG. 12. Experimental and calculated in-band γ-ray yields calculated using the matrix elements from the data of the Hf(Xe, Xe)Hf and Ta(Hf,Hf)Ta experiments.

TABLE IV. The intrinsic matrix elements $m \equiv \langle K_f|\mathcal{M}\lambda|K_i\rangle = m_0 + \Delta\vec{I}^2 m_1$. Errors for the 6^+ band intrinsic matrix elements were propagated from measured isomer branching ratios. Correlated errors are given for the other bands.

m	ν	m_0	m_1	Comment
$\langle 2^+\|E2\|0^+\rangle$	0	0.266(12) eb	−0.00347(15) eb	$m = 0.252(11)$[a]
$\langle 4^+\|E2\|2^+\rangle$	0	0.45(2) eb		
$\langle 4^+\|E2\|0^+\rangle$	2	9.1×10^{-4} eb	-1.47×10^{-5} eb	±6%
$\langle 4^+\|M1\|0^+\rangle$	3	6.3×10^{-5} μ_N	-9.5×10^{-7} μ_N	±30%
$\langle 6^+\|E2\|4^+\rangle$	0	0.094(3) eb		
$\langle 6^+\|E2\|2^+\rangle$	2	0.00116(10) eb		
$\langle 6^+\|E2\|0^+\rangle$	4	1.57×10^{-6} eb	$-2.10\times^{-8}$ eb	±3.5%
$\langle 6^+\|M2\|8^-\rangle$	0	0.102(9) μ_Nb$^{1/2}$		
$\langle 8^-\|E3\|2^+\rangle$	3	$0.36\ ^{+0}_{-0.07}$ eb$^{3/2}$		Alaga rule[b]
$\langle 8^-\|E3\|0^+\rangle$	5	$0.37\ ^{+0.07}_{-0.01}$ eb$^{3/2}$		Alaga rule[b]

[a]To first order in $\Delta\vec{I}^2$.
[b]For $I_{GSB,\gamma} > 9$ only; reduced matrix elements were attenuated for $I < 8$.

physical constraints on the feeding intensity from the GSB, reasonable upper bounds on the $B(E2)$ values [e.g., 10% of the $B(E2)$ strength of the transitions within the GSB], etc.

It was found during the adjustment of the matrix elements that the majority ($\gtrapprox$ 75%–80%) of the isomer activation comes directly from connections between the GSB and the 17^+ and 16^+ isomer band levels (e.g., Fig. 13), as long as the intrinsic matrix element coupling the GSB and the isomer band does not decrease with increasing spin and reasonable upper limits are imposed on the $B(E2)$ strengths. This means that the activition function (Fig. 14) of the Ta(Hf,Hf)Ta experiment and the $19^+ \rightarrow 18^+$ yield calculated for the Hf(Xe, Xe)Hf experiment could be fit almost independently, an obvious constraint being that a smooth, monotonic trend in the magnitudes of the matrix elements is maintained. A second constraint on the fit is that the matrix elements do not introduce γ-decay feeding strengths greater than the measured upper bounds ($\approx 10^{-4}$ relative to the $8^+_{GSB} \rightarrow 6^+_{GSB}$ yield) on feeding in the Hf(Xe, Xe)Hf experiment.

There was insufficient sensitivity to determine the complete set of matrix elements with correlated errors, but a coherent set of matrix elements with upper limits, some lower limits and diagonal (uncorrelated) errors was found that meets the physical constraints described above. Feeding from the GSB is significant (Fig. 13), but the matrix elements which reproduce the yields are consistent with nonobservation of feeding. In particular, the implied 1% $20^+_{GSB} \rightarrow 20^+_{K=16}$ γ-decay branch is three times smaller than the observable lower limit. The energetically favored high E_γ GSB$\rightarrow$ $K = 16$ transitions could not be observed, due to the lack of available double-γ gates and clean single-γ gates.

For the phases of the matrix elements, the arbitrary choice was made to use the signs of the Clebsch-Gordan coefficients $\langle I_{GSB}16 - \lambda\lambda\lambda|I_{K=16}16\rangle$, borrowed from the SDM model, but the goodness of the fit was found to be insensitive to the relative phases, because feeding is more important than direct

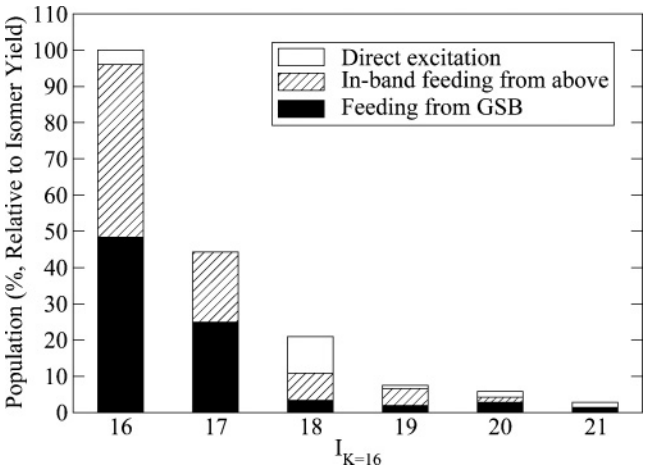

FIG. 13. Population modes of the 16^+ isomer band based on the best fit matrix elements. The fractions of the population of each level attributed to direct Coulomb excitation and γ-decay feeding are given for Hf(Xe, Xe)Hf scattering over 52°–78°.

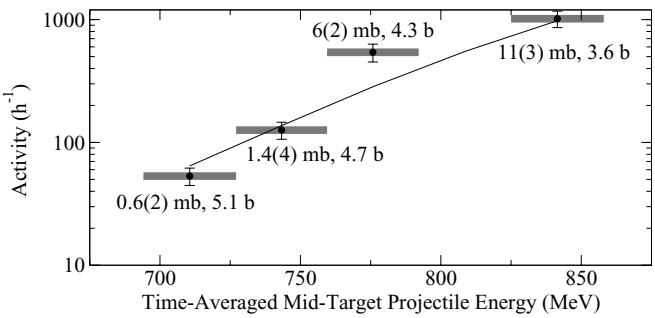

FIG. 14. Measured 16^+ isomer activity versus bombarding energy (points) and predicted activity (line) from the direct fit of the GSB$\rightarrow$ $K^\pi = 16^+$ matrix elements with $\chi^2 = 3.5$. Points are labeled with measured σ_{16^+} (measured) and $\sigma_{Rutherford}$ (calculated for the mean projectile energy in the target). The gray bars indicate the projectile energy range in the targets.

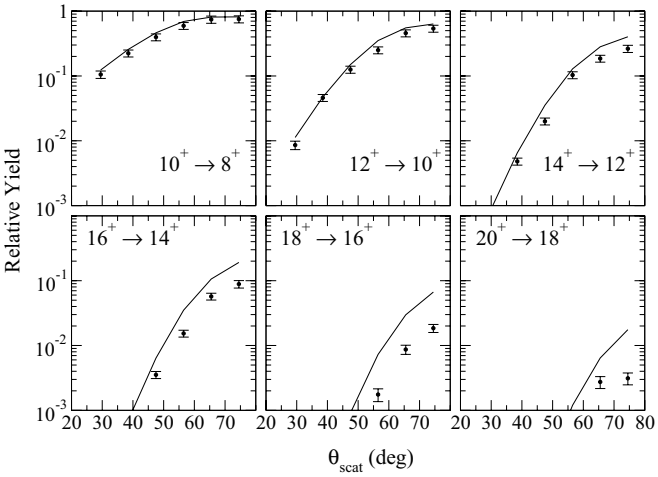

FIG. 15. Measured GSB yields (points) and calculated yields (lines) from the best fit matrix elements.

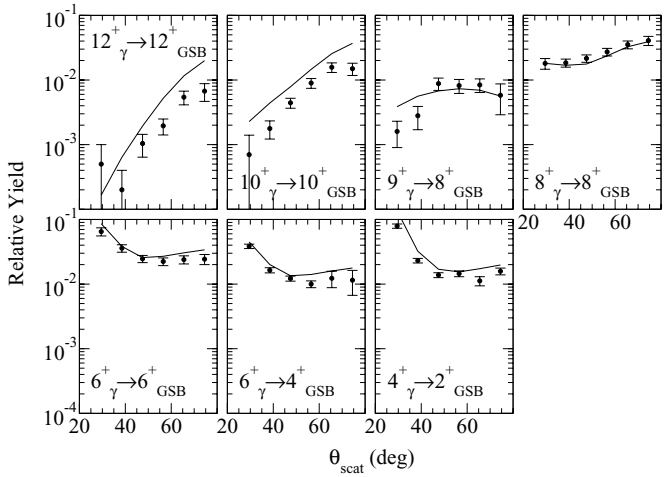

FIG. 16. Measured γ-band to GSB yields (points) and calculated yields (lines) from the best fit matrix elements.

population in the case of the 16^+ isomer activation and the $19^+_{K=16}$ level yield.

IV. RESULTS

A. The ground-state band

The population of the GSB via heavy-ion induced Coulomb excitation is insensitive to the quadrupole moments of the lowest-spin levels, so only $E2$ matrix elements connecting the 6^+ through 18^+ states were adjusted individually. Allowing the $E2$ matrix element connecting each pair of GSB levels, coupled to the static moment of the upper level, to vary independently resulted in a seven-parameter fit of the intrinsic quadrupole moments for the 6^+ through 18^+ states. The intrinsic quadrupole moment for transitions between GSB states $\sqrt{\frac{5}{16\pi}}eQ_0$ is nearly constant at 2.164(10) eb, with deviations of $\leqslant$1.5% between the ground state and the 18^+ state. Calculated GSB yields reproduced by the fit are presented in Fig. 15. Up to $I \approx 16^+$, the agreement between the measured and calculated yields is good, but the calculated yields are higher than the measurements for higher spin. The deviation occurs at the highest states populated, where the only observable yields are at unsafe scattering angles, where destructive nuclear interference could be a significant factor. Regardless of the cause, the deviations at the top of the GSB are not detrimental to the rest of the analysis. The results shown in Fig. 15 are a small subset of the GSB, γ band, and 4^+ band yields used in the fit and do not represent the overall systematic deviation in the GSB yields at the χ^2 minimum.

B. The $K^\pi = 2^+$ γ band

The lowest levels of the γ band were populated nearly to the 10% level in the Hf(Xe, Xe)Hf experiment, relative to the $8^+_{GSB} \rightarrow 6^+_{GSB}$ yield. Typical results from the γ-band fit are shown in Figs. 16 and 17. The overall agreement between the measured and calculated yields for a wide range of spin, multipolarity, and scattering angles is remarkable, considering that the γ-band data were fit with only one parameter to describe the connection between the GS and γ bands using the Alaga rule with the a first-order Mikhailov term. The only significant disagreements (by factors of $\approx$2–5) are in the intraband transition yields, where errors in the branching ratios and the difficulty in measuring branching ratios for higher spin may have led to an inaccurate extrapolation of the Mikhailov term in the matrix element.

C. The $K = 4^+$ band

The SDM model of Bohr and Mottelson [Eq. (1)] for K-forbidden transitions was used to reduce the number of parameters in fitting the $E2$ and $M1$ matrix elements coupling the GSB ($K = 0^+$) and the $K = 4^+$ band (Fig. 18). The matrix elements are given by

$$\begin{aligned}\langle K_f I_f || M(\lambda) || K_i I_i \rangle &= N\sqrt{2I_i+1}\langle I_i K_f - \lambda\lambda\lambda | I_f K_f \rangle \\ &\times \sqrt{\frac{(I_i - K_i)!(I_i + K_i + \nu)!}{(I_i - K_i - \nu)!(I_i + K_i)!}} \\ &\times \langle K_f | m_{\Delta K=\lambda+\nu,\mu=\lambda} | K_i \rangle, \end{aligned} \quad (1)$$

where the normalization N is $\sqrt{2}$ for $K_i = 0$ and 1 for $K_i \neq 0$. (The Mikhailov term makes $\langle K_f | m_{\Delta K=\lambda+\nu,\mu=\lambda} | K_i \rangle$

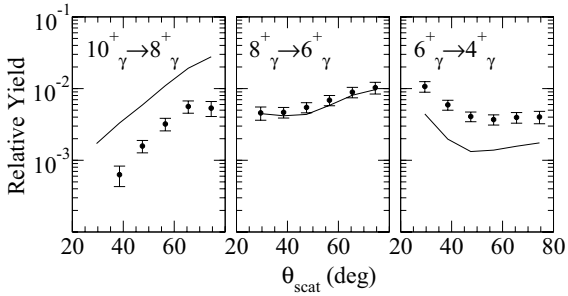

FIG. 17. Measured γ-band to γ-band yields (points) and calculated yields (lines) from the best fit matrix elements.

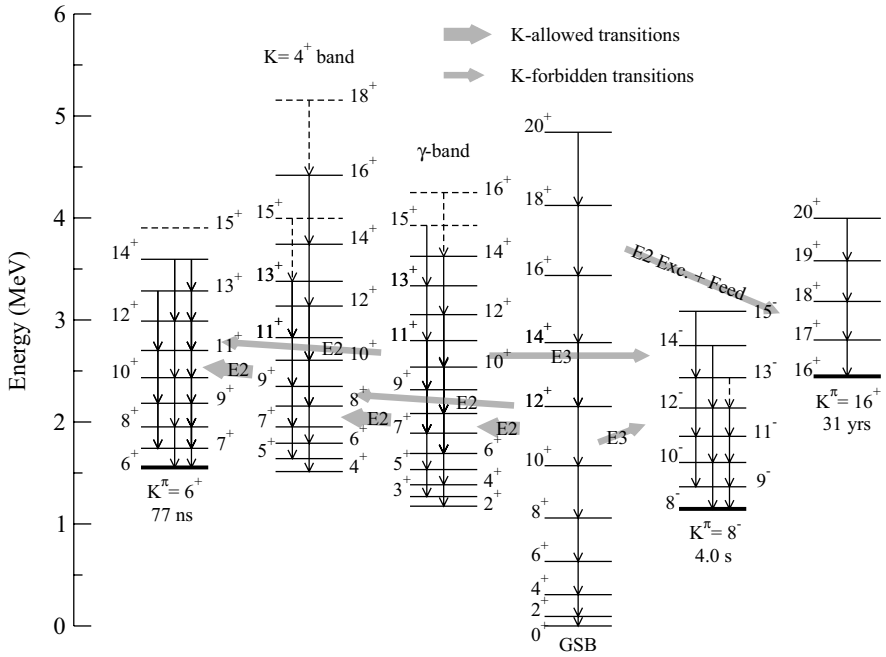

FIG. 18. A schematic representation of the population paths to the three isomer bands. The narrow and wide arrows represent band → band transitions.

linear in $\vec{I}_f^{\,2} - \vec{I}_i^{\,2}$.) Interband $M1$ matrix elements were included, based on known branching and mixing ratios [34]. Four quantities were adjusted in the χ^2 search: $\langle K = 4^+|E2|K = 2^+\rangle$, $\langle K = 4^+|E2|K = 0^+\rangle$, $\langle K = 4^+|M1|K = 0^+\rangle$, and $\langle K = 2^+|E2|K = 0^+\rangle$. The ratio $\langle K = 4^+|E2|K = 0^+\rangle/\langle K = 4^+|M1|K = 0^+\rangle$ was fixed by branching ratios as a single parameter in the fit.

The value of χ^2 was minimized for two relative phases of the $K = 2^+ \xrightarrow{E2} K = 4^+$ and $K = 0^+ \xrightarrow{E2+M1} K = 4^+$ excitations, giving $\chi^2 = 0.83$ for the more destructive choice in the backward angles (phase "D") and $\chi^2 = 1.09$ for the more constructive choice (phase "C"), shown in Figs. 19 and 20. The interference is highly destructive (≈75%) at the χ^2 minimum for either choice of phase, owing to the relative phases of the Clebsch-Gordan coefficients in the SDM and Alaga systematics. The Alaga rule (for K-allowed transitions) and the SDM model (for K-forbidden transitions) simultaneously reproduced the many features of the 4^+ band yield data—using reasonable reduced transition probabilities ($\lesssim$10 W.u.), even for the high-spin states.

An earlier analysis of the present fit results [4] concluded that the 4^+ band was populated predominantly by a two-step process from the GSB, through the γ band. A more systematic analysis of the effect of each intrinsic matrix element indicates that strong interference effects actually make the GSB→ 4^+ and GSB→ γ-band→ 4^+ paths approximately equal in importance. The less destructive sign choice results in a smaller value of $\langle 4^+|E2|2^+\rangle$ at the χ^2 minimum, a corresponding ≈30% reduction in the $B(E2; K = 2 \to K = 4)$ strength and an intrinsic moment ratio of $\langle 4^+|E2|2^+\rangle/\langle 2^+|E2|0^+\rangle = 1.44(9)$, where the harmonic limit is $\sqrt{2}$. However, this choice of phase is less accurate in its overall reproduction of the behavior of the γ-ray yields as a function of scattering angle (Figs. 19 and 20). In addition, this choice of phase

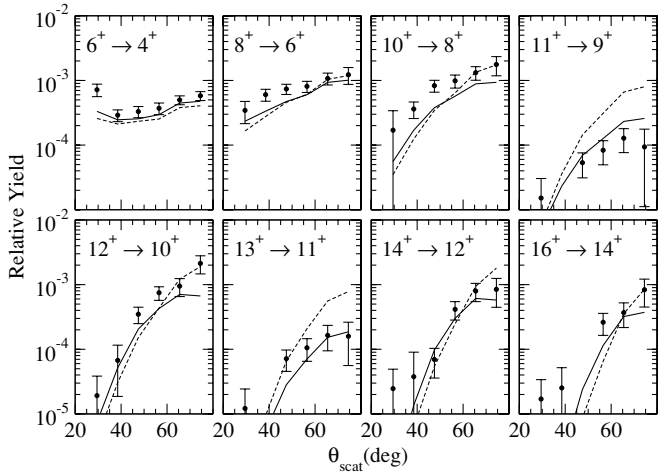

FIG. 19. Measured and calculated $K^\pi = 4^+$ intraband yields showing interference effects. Phases "D" and "C" of the $K = 2^+ \to K = 4^+$ and $K = 0^+ \to K = 4^+$ intrinsic matrix elements are given by the solid and dashed lines, respectively (see text).

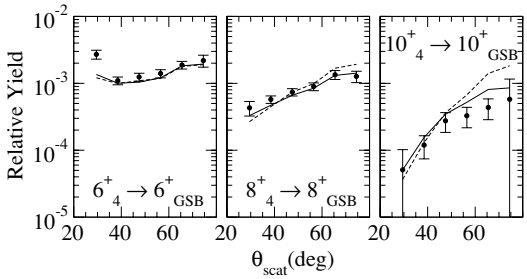

FIG. 20. Measured and calculated interband yields for the 4^+ band. Phases "D" and "C" of the $K = 2^+ \to K = 4^+$ and $K = 0^+ \to K = 4^+$ intrinsic matrix elements are given by the solid and dashed lines, respectively (see text).

gives a ≈15% greater, though not physically unreasonable, $\langle 4^+|E2|\mathrm{GSB}\rangle$ matrix element at the χ^2 minimum.

The more destructive relative phase of the $\langle 4^+|E2|\gamma\rangle$ matrix element with respect to $\langle 4^+|E2|\mathrm{GSB}\rangle$ gives the best overall agreement with the intraband and interband yield data. Some calculated yields rise above the measured data, but the more destructive phase reproduces the complicated yield vs. θ_{scat} slope features remarkably well (Figs. 19 and 20).

The matrix elements for K-allowed transitions between the GSB, the γ band and the 4^+ band reproduce the data well, verifying that the Alaga rule, with an added Mikhailov coupling term where necessary, is sufficiently accurate for describing the K-allowed matrix elements coupling to the high-K bands, i.e., the 6^+ band. The SDM matrix elements were successful in the Coulomb excitation calculations for the population of the 4^+ band from the GSB, showing that the model is useful for low K and low spin. Although the $\sqrt{\frac{(I_1-K_1)!(I_1+K_1+n)!}{(I_1-K_1-n)!(I_1+K_1)!}}$ term in Eq. (1) will behave pathologically for high spin, where the perturbation breaks down, the SDM description predicts physically reasonable matrix elements as long as it is applied to levels having spin I not large compared to K.

D. The $K^\pi = 8_1^-, 8_2^-$ bands

Coulomb excitation calculations showed that only $E3$ matrix elements coupling the GSB and the $K^\pi = 2^+\gamma$ band to the 8^- bands (Fig. 18) can reproduce the measured population strengths of the $K^\pi = 8^-$ bands with smoothly varying, reasonable $B(E3)$ values $\lesssim$1 W.u. Intermediate steps through bands populated below the 10^{-2} level were ineffective, leaving the GSB and the γ band as the only viable candidates to populate the 8^- bands. The 8^- isomer can decay to the 8^+_{GSB} level via an $E1$ or $E3$ transition and to the 6^+_{GSB} level via an $E3$ transition, so that its long lifetime ($t_{1/2} = 4s$) puts a very small upper limit on the $E1$ and $E3$ matrix elements that can populate the 8_1^- isomer state from the GSB. Because it is not possible to populate the 8^- bands to the measured strength without a strong GSB contribution, the GSB→ 8_1^- matrix elements must increase rapidly with increasing spin. For this reason, the $\langle 8^-\|E3\|\mathrm{GSB}\rangle$ matrix elements were attenuated so that $B(E3; K = 0 \rightarrow K = 8)$ decreased by approximately an order of magnitude per unit of spin as I_{GSB} decreased from $10\hbar$ to $6\hbar$ (Fig. 21). A similar attenuation was applied to the $\langle 8^-\|E3\|K^\pi = 2^+\rangle$ matrix elements.

Calculations using a single K admixture in the GSB and in the γ band gave the best agreement in terms of intraband γ-ray yields, isomer cross section, and reasonable $B(E3)$ strengths. Fitting the measured intraband yields with the SDM model more accurately reproduced the absence of population staggering between odd and even spin levels in the isomer band data, whereas fits of an intrinsic matrix element in the Alaga rule produced more staggering, regardless of the particular admixture used. However, the SDM model fails in the case of the 8^- band, because the high degree of forbiddenness causes some matrix elements to take unphysically large values at high spin, some ineffective transitions taking values of ∼100 W.u. at the χ^2 minimum. The slope of calculated yield versus scattering angle was overpredicted by the SDM model by about a factor of 3 with respect to the Alaga rule calculations.

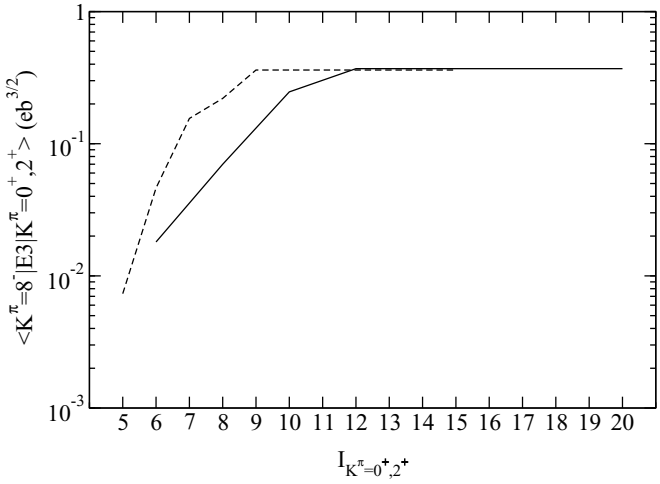

FIG. 21. Values of the intrinsic matrix elements $\langle K^\pi = 8^-_{1,2}|E3|K^\pi = 0^+\rangle$ (solid line) and $\langle K^\pi = 8^-_{1,2}|E3|K^\pi = 2^+\rangle$ (dashed line) vs. spin in the $K = 0, 2$ bands. Both $\langle K^\pi = 8^-_{1,2}|E3|K^\pi = 0^+\rangle$ and $\langle K^\pi = 8^-_{1,2}|E3|K^\pi = 2^+\rangle$ were fit as a single parameter. The intrinsic matrix elements for $I_{K=0,2} \geqslant 12, 9$ were held to a single value. The plotted values correspond to $B(E3; 12^+_{K=0} \rightarrow 15^-_{K=8}) = 1.7$ W.u. and $B(E3; 9^+_{K=2} \rightarrow 12^-_{K=8}) = 2.9$ W.u. using the Alaga rule as described in the text. The Weisskopf unit taken in the *upward* direction is $B(E3; 0^+ \rightarrow 3^-)_W = 0.0132\ \mathrm{e^2b^2}$.

Intraband $M1$ moments and interband $E2$ and $M1$ intrinsic matrix elements connecting the two 8^- bands were derived from the data of Smith [47] and Mullins [32,42], which gave $g_K - g_R = 0.51(5)$ for the 8_1^- band, assuming the same quadrupole moment as that of the GSB (Sec. V A). A value of $g_K - g_R = 0.32(4)$ was calculated for the second 8^- band from branching ratios of Mullins [42]. The interband intrinsic matrix element $\langle K = 8_2^-|E2|K = 8_1^-\rangle = 0.17(3)$ eb was calculated from the only known ratio of intraband/interband $E2$ γ intensities for the 8^- bands [47]. This gave $\langle K = 8_2^-|M1|K = 8_1^-\rangle = 1.10(6)\ \mu_N$. The limited data on the 8_2^- band necessitated locking $\langle 8_1^-|E3|\mathrm{GSB}\rangle = \langle 8_2^-|E3|\mathrm{GSB}\rangle$ as one parameter and $\langle 8_1^-|E3|\gamma\rangle = \langle 8_2^-|E3|\gamma\rangle$ as a second parameter in the χ^2 minimization. Both 8^- bands were populated to approximately equal strengths, so within the precision of the measured yields of the 8^- bands, this is a good approximation. The gyromagnetic ratios and the $\langle 8_2^-|\mathcal{M}\lambda|8_1^-\rangle$ matrix element were held constant.

When the second 8^- band at 1479 keV was included in the calculations, γ decay feeding from the 8_2^- band to the 8^- isomer band reduced the staggering in the calculated yields, so that the Alaga rule fits, using $K = 5^+$ admixtures in the low-K bands, gave good results with $\langle 8^-|E3|\gamma\rangle = 0.36\ ^{+0.00}_{-0.06}\ \mathrm{eb^{3/2}}$ and $\langle 8_1^-|E3|\mathrm{GSB}\rangle = 0.37\ ^{+0.07}_{-0.01}\ \mathrm{eb^{3/2}}$. From these parameters and the forced attenuation at low spin, the Alaga rule gave matrix elements corresponding to $B(E3; K_i \rightarrow K = 8)$ values that range from 10^{-4} to 4 W.u. for the GSB connections, except for the very small $\langle I_{K=8}\|E3\|6^+_{K=0}\rangle$ and $\langle I_{K=8}\|E3\|8^+_{K=0}\rangle$ matrix elements, which were effectively set to zero. $B(E3)$

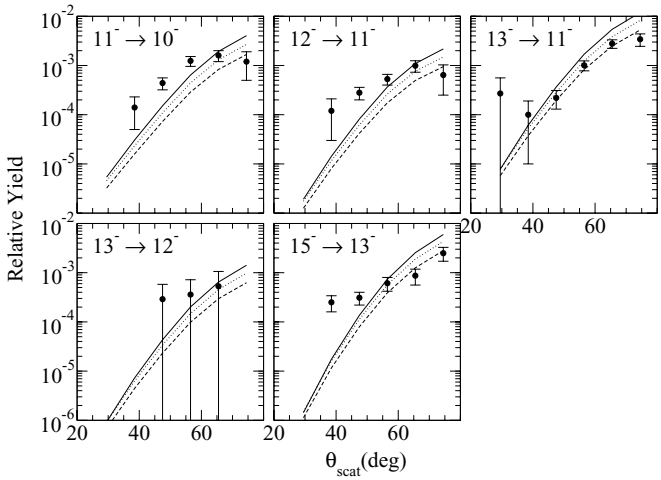

FIG. 22. Intraband yields of the 8^- isomer band and calculated yields from the best fit: total calculation (solid line), calculation for the γ-band$\rightarrow 8^-$ path only (dotted line) and calculation for the GSB$\rightarrow$ 8^- path only (dashed line).

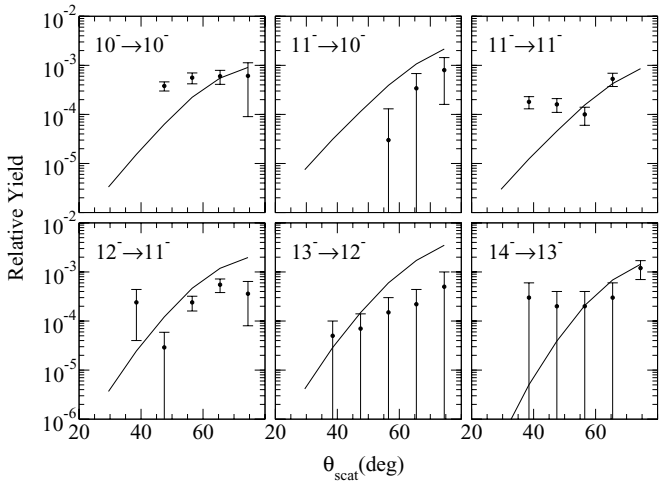

FIG. 23. Interband yields for γ decays from the upper 8^- band at 1479 keV to the 8^- isomer band and calculated yields from the best fit (solid line).

values for the γ-band$\rightarrow 8^-$ band transitions ranged from 7×10^{-4}, as a result of the attenuation applied at low spin in the γ band, to 4 W.u. at high spin. [In the present discussion, the Weisskopf unit is taken in the *upward* or excitation direction as $B(E3; 0^+ \rightarrow 3^-)_W = 0.0132\ \mathrm{e^2b^2}$.]

Nearby nuclei with $N \approx 100$ are characterized by typical octupole strengths closer to 1 W.u. for the $3^-_1 \rightarrow 0^+_1$ transitions, but the strength of the $3^-_{K=2} \rightarrow 0^+_{\mathrm{GSB}}$ transition in ^{178}Hf has been measured to be 4 W.u. [48], so the maximum values here of $\lesssim$4 W.u. are not unreasonably large. Because the calculated yields are not extremely sensitive to reduction of the few matrix elements with $B(E3) \approx 4$ W.u., additional data might in fact show that the largest matrix elements are actually smaller than those given by the Alaga rule. Figures 22 and 23 display the agreement between the measured and calculated 8^- bands yields. The calculated yields for the $K = 5$ admixture put an upper limit on the population of the 8^- bands by γ-decay feeding from the low-K bands of $\lesssim 10^{-5}$ of the total yield. Admixtures other than $K = 5$ in the low-K bands give very similar results, so the same general conclusions would be drawn from any postulated admixture, but in the absense of any contradictory information, it was assumed that the lowest K admixtures enter the GSB wave function first and dominate the GSB$\rightarrow 8^-$ transitions.

From the χ^2 fit, the population was calculated to be $\approx$50–60% from the γ band, depending on the scattering angle range. Coulomb excitation calculations showed that the 10^+_{GSB} level is responsible for the largest fraction of the population from the GSB, regardless of the particular model chosen, and is mostly determined by the experimental parameters (beam energy, etc.). The $10^+_{\mathrm{GSB}} \rightarrow 12^-_{K=8}$ and $10^+_{\mathrm{GSB}} \rightarrow 13^-_{K=8}$ excitations to the isomer band are the most effective, with the excitation of the unnatural parity 12^- state competing because of the 4 times greater $B(E3)$ value of the Alaga rule systematics for $K = 5$ to $K = 8$ coupling.

Hamilton [8] and Xie [9] have measured the probability of exciting the 8^- isomer from the ground state by Coulomb excitation. Xie *et al.* measured a lower cross section than Hamilton *et al.*, and calculations of the cross sections for these two experiments based on the matrix elements from the present work lie between the measurements of Hamilton and Xie (Table V).

Hamilton *et al.* achieved the first Coulomb excitation of the $K = 8^-$ isomer in a 35-mg/cm^2 ^{178}Hf target with 594 MeV ^{136}Xe ions. By comparing the beam-off γ-ray yield of the GSB $8^+ \rightarrow 6^+$ transition to the beam-on yield, the isomer population was measured relative to the 8^+_{GSB} yield at "$\approx$0.9%" (Table V). The present results were used to simulate the Hamilton experiment, integrating over 4π sr scattering, giving a calculated isomer decay feed of 0.5%, i.e., within a factor of 2 of the Hamilton result.

Xie *et al.* Coulomb excited a 0.5-mg/cm^2 ^{178}Hf target with ^{130}Te beams at 560, 590, and 620 MeV and counted delayed GSB γ-ray yields. A simulation of the Xie experiment based on the present results predicts an absolute cross section σ_{8^-} five to six times larger than that reported by Xie *et al.* The present set of model-dependent matrix elements reproduced the measured prompt 8^- isomer band yields with $\chi^2 \approx 1.6$

TABLE V. Comparison of the measurements of Xie *et al.* [9] ^{178}Hf(^{130}Te,^{130}Te)^{178}Hf, thin target] and Hamilton *et al.* [8] [^{178}Hf(^{136}Xe,^{136}Xe)^{178}Hf, thick target] to predictions based on the present best fit matrix elements. The intensity ratio r is defined as $(8^+_{\mathrm{GSB}} \rightarrow 6^+_{\mathrm{GSB}})_{\mathrm{delayed}}/(8^+_{\mathrm{GSB}} \rightarrow 6^+_{\mathrm{GSB}})_{\mathrm{total}}$. The experiments are described in the text.

	560 MeV	Xie *et al.* cross sections (mb) 590 MeV	620 MeV	Hamilton *et al.* r 594 MeV
Meas.	$2.7\ ^{+1.9}_{-1.4}$	$4.3\ ^{+3.4}_{-2.0}$	$7.5\ ^{+6.1}_{-3.2}$	$\approx$0.9%
Calc.	15.7	25.3	37.6	0.5%
$\frac{\text{Calc.}}{\text{Meas.}}$	5.8	5.9	5.0	0.6

and a σ_{8^-} value lying between those of the Xie and Hamilton experiments.

Coulomb excitation calculations were used to rule out significant $E1$ and $E5$ contributions to the population of the $K = 8^-$ bands. Electric dipole transitions between the low-K and $K = 8$ bands would be dominated by $\geqslant 90\%$ γ-decay feeding, even where feeding transitions into the 8^- band have $E_\gamma \approx 300$ keV. $E1$ transitions with reduced transition strengths of the order of 10^{-3} W.u. (comparable to known values in ^{178}Hf [33,49]) could populate the 8^- bands to the measured levels from the GSB or the γ band, but the measured feeding upper limits restrict the $E1$ contribution to $\sim 5\%$ of the measured yields. Assuming a set of extremely large $E5$ matrix elements, 1 W.u. for the $9^-_{K=8} \rightarrow 4^+_{\rm GSB}$ transition, results in predicted 8^- band yields that were more than three orders of magnitude too small, ruling out a significant $E5$ contribution.

E. The $K^\pi = 6^+$ isomer band

Rather than using a χ^2 fit to determine the 6^+ band matrix elements, measured $B(E2)$ values of the 6^+ isomer decays (Table II) were used to extrapolate the matrix elements in the Alaga, Mikhailov, and SDM systematics as appropriate. Coulomb excitation calculations with these matrix elements reproduced the measured in-band yields of the 6^+ band. The matrix element $\langle 6^+|E2|4^+\rangle = 0.094(3)$ eb has been determined from the measured $B(E2)$ value, because the K-allowed transitions between the 4^+ and 6^+ bands should be well-described by the Alaga rule. The $K = 4^+ \rightarrow K = 6^+$ path (Fig. 18) was found to be important in the Coulomb excitation of the 6^+ isomer band (Fig. 24). Measured errors in the reduced transition probabilities for the 6^+ isomer decay branches were used to directly calculate errors in the intrinsic matrix elements (Table IV). Each quoted error represents the sum of several contributions, primarily from the measured γ-ray yields ($\lesssim 10\%$) and the relative γ-ray efficiency ($\approx 5\%$).

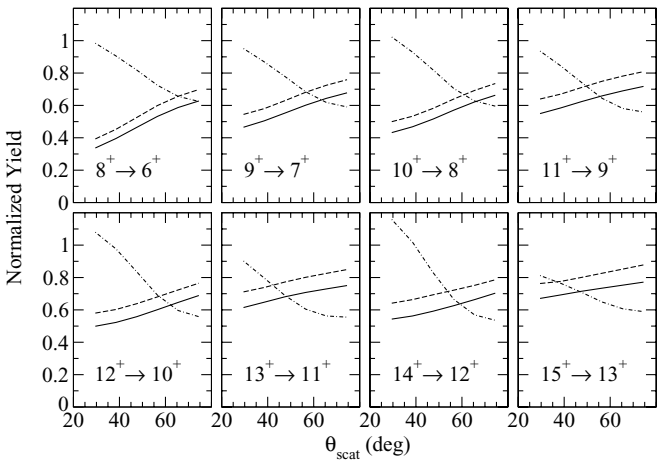

FIG. 24. Calculated 6^+ intraband yields normalized to the total Coulomb excitation calculations, calculated after removing each of three population paths: $\langle 6^+|E2|\gamma\rangle$ (solid), $\langle 6^+|E2|4^+\rangle$ (dashed), $\langle 6^+|E2|\text{GSB}\rangle$ (dashed-dotted).

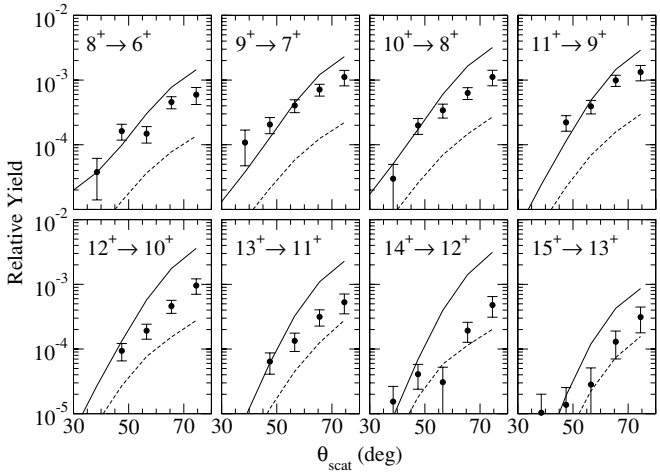

FIG. 25. Intraband $\Delta I = 2$ yields of the 6^+ band for even spin. The solid and dashed lines represent Coulomb excitation calculations from measured $B(E2)$ values for opposite relative phases of the intrinsic matrix elements (see text).

The calculated γ-ray yields are in agreement with the measured γ-ray triples yields for the 6^+ band for safe scattering angles forward of 60°, as shown in Figs. 25 and 26. The contributions of the GSB and the γ band have been determined, insofar as the SDM model [Eq. (1)] correctly describes the K-forbidden transitions, along with the relative phases of the intrinsic matrix elements $\langle K^\pi = 6^+|E2|K^\pi = 2^+\rangle$ and $\langle K^\pi = 6^+|E2|K^\pi = 4^+\rangle$, indicating that constructive interference is required to reproduce the yields. It appears that the γ- and 4^+ band connections together are responsible for >50% of the 6^+ band population at safe scattering angles $\theta^{\rm lab}_{\rm scat} < 52^\circ$ (Fig. 24). Connections with the GSB are responsible for $\leqslant 25\%$ at forward angles, but may be responsible for the majority of the 6^+ band excitation at unsafe scattering angles. The correct phase of the $\langle 6^+|E2|\text{GSB}\rangle$ intrinsic matrix element, relative to the other two population paths, cannot be determined from the present data. The relative significance attributed to connections with the GSB and the γ band depend on the model used,

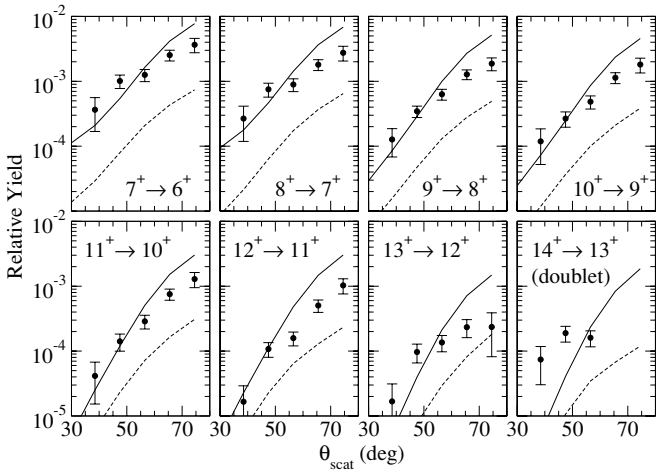

FIG. 26. Intraband $\Delta I = 1$ yields of the 6^+ band for odd spin.

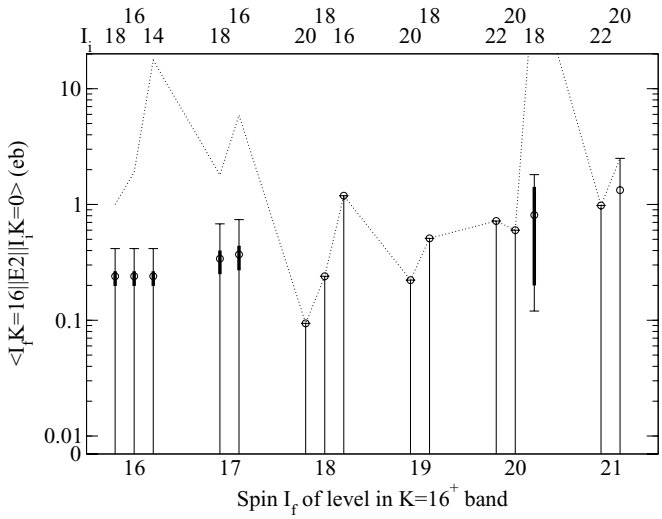

FIG. 27. Final set of matrix elements (magnitudes only) connecting the GSB to the 16^+ isomer band. Matrix elements (circles) are shown with diagonal error estimates (black bars) and upper and lower limits ($\top$ and $\perp$) where they could be determined. The dotted line represents the upper limits on the matrix elements calculated from measured upper limits on feeding.

because the Alaga rule does not describe these K-forbidden transitions.

F. The $K^\pi = 16^+$ band

The best agreement with the slope of the activity vs. the bombarding energy was obtained by setting $\langle 16^+_{K=16}\|E2\|14^+_{\rm GSB}\rangle = \langle 16^+_{K=16}\|E2\|16^+_{\rm GSB}\rangle = \langle 16^+_{K=16}\|E2\|18^+_{\rm GSB}\rangle$. Matrix elements coupled to the $18^+_{K=16}$ state were increased to the feeding limit in the fit. The overall magnitudes of the $17^+_{K=16}$ matrix elements were roughly interpolated between the values of the $16^+_{K=16}$ and $18^+_{K=16}$ ones, continuing the trend of increasing K mixing with increasing spin.

The matrix elements for the $16^+_{K=16}$, $17^+_{K=16}$, and $18^+_{K=16}$ levels given in Fig. 27 were found to be ineffective in populating the $19^+_{K=16}$ level, whose yield was measured in the Hf(Xe, Xe)Hf experiment, so the measured $19^+ \rightarrow 18^+$ yield could be fit independently by adjusting the matrix elements connecting the GSB to the $19^+_{K=16}$, $20^+_{K=16}$, and $21^+_{K=16}$ levels. Because most of the 19^+ population comes from the $\langle 19^+_{K=16}\|E2\|18^+_{\rm GSB}\rangle$ and $\langle 20^+_{K=16}\|E2\|18^+_{\rm GSB}\rangle$ matrix elements, ranges for the other five matrix elements populating the 19^+ level could not be determined, except for upper limits based on feeding. The absolute upper limit of $\langle 20^+_{K=16}\|E2\|18^+_{\rm GSB}\rangle$ was estimated by setting $\langle 19^+_{K=16}\|E2\|18^+_{\rm GSB}\rangle$ to zero and increasing $\langle 20^+_{K=16}\|E2\|18^+_{\rm GSB}\rangle$ until $\chi^2 = \chi^2_{\rm min} + 1$. Correlations with the other five matrix elements were found to be small. Correlated error calculations between the matrix elements $\langle 19^+_{K=16}\|E2\|18^+_{\rm GSB}\rangle$ and $\langle 20^+_{K=16}\|E2\|18^+_{\rm GSB}\rangle$ could not define any lower limit or further restrict the upper limit for $\langle 19^+_{K=16}\|E2\|18^+_{\rm GSB}\rangle$, because the $\langle 20^+_{K=16}\|E2\|18^+_{\rm GSB}\rangle$ matrix element has a higher upper limit and can independently reproduce the measured $19^+ \rightarrow 18^+$ yield with $\chi^2 < \chi^2_{\rm min} + 1$. One lower limit on $\langle 20^+_{K=16}\|E2\|18^+_{\rm GSB}\rangle$ was obtained.

The diagonal (uncorrelated) errors (Fig. 27) were measured in the six matrix elements that provided enough sensitivity for the calculation. The matrix elements for the $16^+_{K=16}$ level were coupled as one parameter and varied until $\chi^2 = \chi^2_{\rm min} + 1$, giving a range of 0.20–0.26 eb. The matrix elements of the $17^+_{K=16}$ level were coupled in an identical error calculation, giving ranges of 0.27 eb $\leqslant \langle 17^+_{K=16}\|E2\|16^+_{\rm GSB}\rangle \leqslant 0.44$ eb and 0.25 eb $\leqslant \langle 17^+_{K=16}\|E2\|18^+_{\rm GSB}\rangle \leqslant 0.40$ eb.

More restrictive upper limits (below the feeding limits) for six matrix elements were obtained, based on the measured activities from the second experiment and the prompt $19^+ \rightarrow 18^+$ yields from the first experiment. These are the six points in Fig. 27 with solid black bars. Since each of the three GSB connections to the 16^+ level contributes approximately the same fraction of the total level population, reducing any two to zero would require a factor of $\approx$3 increase in the $B(E2)$ value ($\sqrt{3}$ in the matrix element) of the third to maintain the observed yield.

The 17^+ level connections contribute about 25% of the total isomer yield (Figure 13). If the 16^+ level connections were reduced to an ineffective level, the 17^+ matrix elements would have to be increased by a factor of about $\sqrt{\frac{1}{0.25}}$. These considerations lead to the upper limits for the first five matrix elements in Table VI and Fig. 27.

Population of the 16^+ isomer due to feeding from the $t_{1/2} = 68\ \mu$s, 14^- isomer at 2573 keV could make a significant contribution to the 16^+ activation, if the 14^- isomer were populated to a strength comparable to the direct excitation of the 16^+ band. The known decay branch to the 16^+ isomer from the 14^- isomer is shown with the known relative intensities in Fig. 28. None of the data sets provided an unambiguous yield from the 14^- isomer band, but a gate on the $15^- \rightarrow 14^-$, 337-keV transition in a prompt-prompt matrix above the safe angle (52°–78°) yielded a peak possibly belonging to the $16^- \rightarrow 15^-$, 355-keV transition, lying in a rich background of coincident peaks. The $18^+_{K=16} \rightarrow 17^+_{K=16}$ yield was measured in the same matrix, although the identities of both peaks were

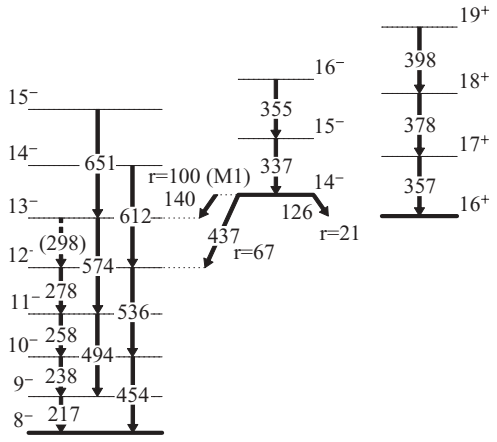

FIG. 28. Previously known levels and decay branches of the 2573 keV 14^- $t_{1/2} = 68\ \mu$s isomer. Relative γ intensities [34] are indicated beside each branch.

TABLE VI. Matrix elements $m = \langle I_f, K = 16^+ \| E2 \| I_i, K = 0^+ \rangle$ and $B(E2; K = 0^+ \rightarrow K = 16^+)$ values for the $\nu = 14$ K-forbidden transitions. Matrix elements were adjusted to reproduce the data from both the Hf(Xe, Xe)Hf and the Ta(Hf,Hf)Ta experiments. Upper and lower bounds are given where they could be determined, along with diagonal errors. *Note: The $B(\mathcal{M}\lambda)$ values in the tables are arbitrarily given in the upward direction, from I_i to I_f. For comparison, the E2 Weisskopf estimate is $B(E2\uparrow)_W = 0.0297\,e^2b^2$.*

GSB$\rightarrow$ $K = 16^+$ band						
I_i	I_f	$B(E2)$ (10^{-3} e^2b^2)	Matrix element (eb)			
			m	Lower limit	Upper limit	Diagonal error range
14	16	2.0	0.24		0.42	0.20–0.26
16	16	1.7	0.24		0.42	0.20–0.26
16	17	4.1	−0.37		0.74	0.27–0.44
16	18	43.	1.19		1.19	
18	16	1.6	0.24		0.42	0.20–0.26
18	17	3.1	−0.34		0.68	0.25–0.40
18	18	1.6	0.24		0.24	
18	19	7.0	−0.51		0.51	
18	20	18.	−0.81	0.12	1.8	0.20–1.4
20	18	0.21	0.094		0.094	
20	19	1.2	−0.22		0.22	
20	20	8.8	0.60		0.60	
20	21	43.	−1.33		2.5	
22[a]	20	11.	0.72		0.72	
22[a]	21	21.	−0.98		0.98	

[a]The 22^+ GSB level has not been found.

not certain at the 10^{-3} level in the two-dimensional data. After correcting for the relative efficiency of the transition energies and internal conversion, the ratio of the populations of the second level in the 16^+ and 14^- isomer bands was found to be $\frac{P_{14^-}}{P_{16^+}} = 0.47$.

Assuming that the 437-keV, $14^-_{K=14} \rightarrow 12^-_{K=8}$ transition is purely $E2$ in character gives the largest estimate of the $14^-_{K=14} \rightarrow 16^+_{K=16}$ partial width calculated from the known 68 μs half-life of the 14^- isomer. Then, the following estimate can be made of the 14^-_{isomer} feeding contribution to the 16^+ isomer state. The known γ-ray intensities and internal conversion coeffients would indicate reduced transition strengths of $B(E3) = 510$ W.u., $B(M2) = 0.014$ W.u., and $B(M4) = 1.5 \times 10^{11}$ W.u. The absurdly high values for the $E3$ and $M4$ possibilities leave M2 as the only realistic multipole character. If the observed 355-keV peak belongs to the $16^-_{K=14} \rightarrow 15^-_{K=14}$ transition (Fig. 28), then a ≈10% decrease in the matrix elements of Table VI would make up for the feeding contribution from the 14^- band.

G. The question of transfer reaction contributions

It can be argued that the isomer bands in question might have been populated in the Hf(Xe, Xe)Hf experiment through transfer reactions involving the ^{177,179}Hf contaminants (4% and 3%, respectively) in the target. The most straightforward test to address this possibility would be to select events containing transitions in ^{178}Hf and compare the relative amounts of Xe isotopes in coincidence. Although this shows no indication of transfer reactions, the background of Doppler-broadened lines of hafnium in the resulting Xe spectra is large and does not allow the observation of small amounts of ^{135}Xe and ^{137}Xe that would result from potentially significant transfer reactions (Fig. 29). An upper limit on the rate of the transfer reaction ^{178}Hf(^{136}Xe,^{135}Xe)^{179}Hf was set experimentally and then used to estimate the rate of ^{177}Hf(^{136}Xe,^{135}Xe)^{178}Hf transfer.

The spectra of Fig. 29 for safe scattering angles $25^\circ \leqslant \theta^{\text{lab}}_{\text{scat}} \leqslant 52^\circ$ contain no transitions of Xe isotopes other than ^{136}Xe, when gated on "random coincidences" [Fig. 29(a)] with two arbitrary energies between the known ^{178}Hf peaks, when gated on two known GSB transitions [Fig. 29(b)] and on the known transitions of the ^{179}Hf GSB [Fig. 29(c)]. An upper limit on ^{178}Hf(^{136}Xe,^{135}Xe)^{179}Hf transfer reactions was set using the only possible ^{135}Xe transition (288 keV) observed in coincidence with a double gate on ^{178}Hf GSB transitions [Figs. 29(c) and 30(c)]. In the safe Coulomb excitation region, $25^\circ < \theta^{\text{lab}}_{\text{scat}} < 52^\circ$, where significant populations of the $K^\pi = 6^+_{\text{isom}}, 8^-_{\text{isom}}$ bands are already seen, an upper limit on ^{177}Hf(^{136}Xe,^{135}Xe)^{178}Hf transfer was set at 10^{-5} of the ^{178}Hf GSB excitation. The neutron transfer cross sections reach a maximum at $Q = 0$, and the Q values of the ^{177}Hf(^{136}Xe,^{135}Xe)^{178}Hf ($Q = -0.4$ MeV) and ^{178}Hf(^{136}Xe,^{135}Xe)^{179}Hf ($Q = -1.9$ MeV) reactions differ by only 1.5 MeV, so the two transfer cross sections are expected to be comparable [50]. Assuming that they are approximately equal, the upper limit on ^{177}Hf(^{136}Xe,^{135}Xe)^{178}Hf reactions in the 4% ^{177}Hf impurity is $\sim\frac{1}{10}$ of the observed 16^+ isomer

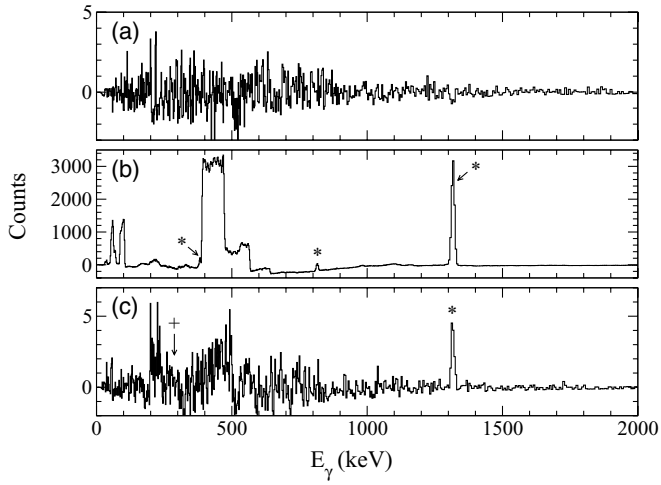

FIG. 29. Resultant background-subtracted spectra, Doppler-corrected for Xe-like particles, from gates in an asymmetric Xe-Hf-Hf cube in the safe region, $25^\circ \leqslant \theta^{\rm lab}_{\rm scat} \leqslant 52^\circ$. (a) Gated on "random coincidences" (see text). (b) Gated on the GSB of ^{178}Hf. (c) Gated on the GSB of ^{179}Hf. The asterisk indicates ^{136}Xe transition energies. The plus sign indicates the position of the unobserved ^{135}Xe transition at 288 keV.

band yield in the unsafe region $52^\circ < \theta^{\rm lab}_{\rm scat} < 78^\circ$. Transfer in the unsafe region should be greatest at larger $\theta^{\rm lab}_{\rm scat}$ angles, and because no transfer is observed in the safe region, it would be unlikely to find a significant transfer cross section near 52°, even in the unsafe region, where strong isomer populations are already seen. Moreover, transfer must be divided among several bands, and transfer to a four-quasiparticle state (e.g., the $16^+_{\rm isom}$ band) is very unlikely, because breaking a second pair of nucleons is a higher-order effect. But the most compelling argument against significant population of the

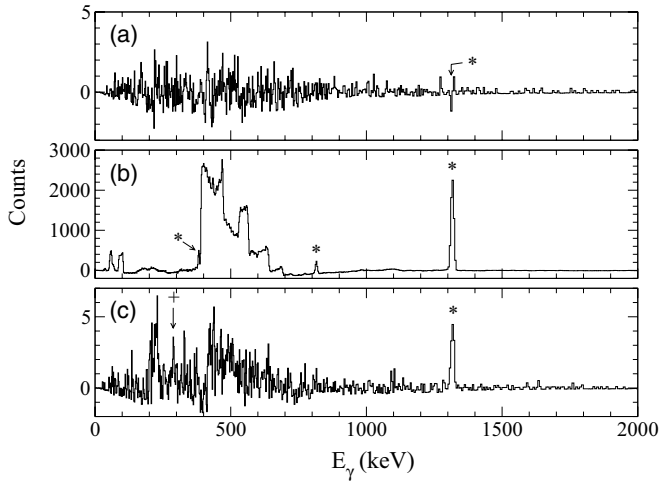

FIG. 30. Resultant background-subtracted spectra from gates in an asymmetric Xe-Hf-Hf cube in the unsafe region, $52^\circ \leqslant \theta^{\rm lab}_{\rm scat} \leqslant 78^\circ$. (a) Gated on "random coincidences" (see text). (b) Gated on the GSB of ^{178}Hf. (c) Gated on the GSB of ^{179}Hf. The asterisk indicates ^{136}Xe transition energies. The plus sign indicates the position of a possible ^{135}Xe transition at 288 keV.

isomers by transfer reactions is in the results of the ^{178}Hf beam activation experiment, where the 16^+ isomer was activated with significant cross sections 27% below the Coulomb barrier, consistent with the Coulomb excitation function (Fig. 14).

H. Summary of results

Three distinctly different paths have been determined that Coulomb excite the $K^\pi = 6^+, 8^-$, and 16^+ isomer bands. Multiple-step excitations populate the 6^+ band via the γ and 4^+ bands primarily, using both K-allowed and K-forbidden transitions. The 8^- bands are excited directly from the γ band and the GSB by highly K-forbidden $E3$ transitions. The Hf(Xe, Xe)Hf data are consistent with direct γ-decay feeding into the 16^+ band; however, the additional data provided by the Ta(Hf,Hf)Ta activation experiment leads to a departure from the SDM model, and direct excitation is not insignificant in the population of all of the 16^+ isomer band states. These three results, as well as those for the γ and 4^+ bands have shown that the SDM model is a useful approximation for low spin and low forbiddenness, ν.

The SDM model could not simultaneously reproduce the 16^+ data of the first and second experiments, even with unrealistically large matrix elements. The population of the isomer band head was found to proceed primarily, ≈75%, by γ-decay feeding from the GSB to the 16^+ and 17^+ levels. A nearly constant magnitude of the matrix elements was required to reproduce the entire data set from both experiments. Figure 14 shows the agreement between the calculated and measured isomer activity from the Ta(Hf,Hf)Ta experiment with $\chi^2 = 3.5$. The slope and magnitude are reproduced, the largest χ^2 contribution coming from the third target. The agreement with the measured $19^+ \rightarrow 18^+ \gamma$-ray yield ($\chi^2 = 1.9$) of the Hf(Xe, Xe)Hf experiment is shown in Fig. 12. The present set of matrix elements simultaneously reproduced both the measured Ta(Hf,Hf)Ta activation and the $19^+ \rightarrow 18^+$ yield.

V. DISCUSSION

A. Electromagnetic properties

The principal parameters relevant to intraband and interband EM transition probabilities are presented below for the $K^\pi = 0^+, 2^+, 4^+, 6^+, 8^-, 14^-$, and 16^+ bands studied. Measurements of the two-quasiparticle configurations in the 6^+ and 8^- bands are discussed. The interband intrinsic and reduced matrix elements and a comparison of isomer cross sections are given in Tables IV, VI, and VII, respectively.

1. The GSB

The intrinsic quadrupole moment of the GSB was measured for $I \rightarrow I \pm 2$ transitions, assuming static moments corresponding to a prolate deformation, giving $\sqrt{\frac{5}{16\pi}} e Q_0 = 2.164(10)$ eb, constant within 1.5% between levels up to spin 18^+, despite the strong up-bend observed in the moment of inertia. The present value is in agreement with the results of

TABLE VII. Summary of calculated (top) and measured (bottom) cross sections for the isomers. (The cross sections for the Xe beam experiment were integrated using the intrinsic matrix elements fitted to the online data.) The total Rutherford cross sections are 11.0 b (top) and 3.6 b (bottom, 86% E_{barrier}) both calculated for the mean projectile energy in the target.

^{178}Hf(^{136}Xe,^{136}Xe)^{178}Hf (calc.) $\frac{E_{\text{beam}}}{E_{\text{barrier}}} = 96\%$, $25^\circ \leqslant \theta_{\text{Xe}} \leqslant 78^\circ$			
Level	Model/Fit	σ_{fit} (mb)	$\sigma_{\text{fit}}/\sigma_{\text{Ruth}}$
2^+_{GSB}	Rotor	9690(90)[a]	0.900(8)
6^+_{isom}	SDM model	6.4(11)[b]	$5.9(10) \times 10^{-4}$
8^-_{isom}	Alaga, total	16(4)[a]	$15(4) \times 10^{-4}$
	Alaga, GSB contrib.	6.5	6.0×10^{-4}
	Alaga, $\gamma \rightarrow 8^-$ contrib.	10.3	9.6×10^{-4}
14^-_{isom}	Upper limit	<2[c]	$< 2 \times 10^{-4}$
16^+_{isom}	Fit	4(2)[d]	$4(2) \times 10^{-4}$
Ta(^{178}Hf,^{178}Hf)Ta (meas.) $40^\circ \leqslant \theta_{\text{Hf}} \leqslant 180^\circ$			
Level	$\frac{E_{\text{beam}}}{E_{\text{barrier}}}$ (%)	σ_{meas} (mb)	$\sigma_{\text{meas}}/\sigma_{\text{Ruth}}$
16^+_{isom}	86	11(3)[e]	$30(8) \times 10^{-4}$
16^+_{isom}	80	6(2)[e]	$14(5) \times 10^{-4}$
16^+_{isom}	76	1.4(4)[e]	$3.0(8) \times 10^{-4}$
16^+_{isom}	73	0.6(2)[e]	$1.2(4) \times 10^{-4}$

[a]Uncertainty from the correlated error calculations.
[b]Uncertainty from the measured 6^+ branching ratios.
[c]Upper limit.
[d]Uncertainty from the largest diagonal error in the fitted set of matrix elements.
[e]Cross section measured directly.

previous lifetime measurements of the 2^+ state, $\sqrt{\frac{5}{16\pi}}eQ_0 = 2.17(3)$ eb [51], and indicates a quadrupole deformation parameter of $\beta_2 \approx 0.25$ [7,52].

2. The γ band at 1175 keV

The intrinsic quadrupole moment of the γ band was measured, giving $\sqrt{\frac{5}{16\pi}}eQ_0 = 2.21(8)$ eb, in agreement with the GSB value. A linear dependence of the interband intrinsic matrix element $\langle\gamma|E2|\text{GSB}\rangle$ on $\Delta\vec{I}^2$ was included, adjusted to simultaneously fit several previous measurements of $B(E2; I_\gamma \rightarrow I_{\text{GSB}})$ [34,43] and the present measured branching ratios. The overall effect of the rotational-vibrational coupling is a ≈10% increase in the interband $B(E2; \text{GSB} \rightarrow K = 2)$ strength between the 2^+ and 16^+ states of the γ band, over the Alaga-rule systematics. The $B(E2; \text{GSB} \rightarrow \gamma)$ values resulting from the fit reached a maximum of 4 W.u. The present measurement of the $\langle\gamma|E2|\text{GSB}\rangle$ matrix element (Table IV) is comparable to values for other nuclei in the $A \approx 180$ mass region [53]. The population of the γ band was found to be insensitive to both the intraband and interband $M1$ intrinsic matrix elements, within the experimental error.

3. The 4+ band at 1514 keV

As in the $K^\pi = 0^+, 2^+$ bands, a prolate rigid rotor was assumed in fitting the intrinsic transition quadrupole moment of the 4^+ band, giving a value of $\sqrt{\frac{5}{16\pi}}Q_0 = 2.07(10)$ eb, consistent with the GSB and the γ band. The 4^+ band has been tentatively identified as the two-phonon γ-vibrational band [54,55], based largely on the similarity in the dynamic moments of inertia of the $K^\pi = 2^+$ and $K^\pi = 4^+$ bands. For an isolated harmonic vibrator system, the ratio of the level energies $\frac{E_{2-\text{phonon}}}{E_{1-\text{phonon}}} \approx 2$ is expected, compared to 1.29 in the present case. The Alaga rule fit gave a ratio of intrinsic matrix elements of $\frac{\langle K=4^+|E2|K=2^+\rangle}{\langle K=2^+|E2|K=0^+\rangle} = 1.77(11)$, compared to the expectation of $\sqrt{2}$ for pure harmonic vibrators [53]. The energy of the 2^+ band head is in line with the expectation of ≈1 MeV for a harmonic oscillator with $A = 178$, and the intrinsic matrix element $\langle K = 2^+|E2|K = 0^+\rangle = 0.252(11)$ is similar to the values measured in ^{156}Gd, ^{160}Dy, and ^{168}Er [53], whereas $\langle K = 4^+|E2|K = 2^+\rangle = 0.45(2)$ eb is closer to values for heavier osmium nuclei [53]. Assuming that the 4^+ state is indeed a two-phonon γ-vibration, then there is significant anharmonicity, implied by both the energy ratio and the ratio of intrinsic moments.

Previous attempts to measure the lifetime of the $4^+_{K=4}$ state have succeeded in setting a lower limit of 0.94 ps [37], and the intensity ratios of its K-forbidden and K-allowed γ decays have been measured, along with a single $E2/M1$ mixing ratio [41]. The present Xe beam experiment provided an *upper* limit on the $4^+_{K=4}$ lifetime of ≈4 ns from the width ΔE of the Doppler-corrected 1207 keV $4^+_{K=4} \rightarrow 4^+_{K=0}E_\gamma$ peak and particle time-of-flight considerations (not to be confused with a Doppler lineshape measurement). For states with lifetimes greater than 1 ns and recoil velocities of $\beta \geqslant 0.05$, the measured particle-γ opening angle $\theta^{\text{lab}}_{\text{p},\gamma}$ deviates from the true laboratory angle because of the large recoil distance when the γ ray is emitted, and the resulting increase in $\frac{\Delta E}{E}$. In the limit as the lifetime $\tau \rightarrow 0$, the resolution is $\frac{\Delta E}{E} \approx 0.5\%$. The measured FWHM of the 1207 keV peak, $\frac{\Delta E}{E} = 0.8\%$, leads to an upper limit on the lifetime of the 4^+ state of ≈4 ns. The limits 0.94 ps $< \tau_{4^+_{K=4}} <$ 4 ns suggest approximate bounds for the $\nu = 2$ K-forbidden matrix elements connecting the GSB and 4^+ bands, corresponding to reduced hindrance values of approximately $1 < f_\nu < 90$. The $4^+_{K=4}$ lifetime calculated from the present Coulomb excitation data is 90 ps, and the calculated $E2$ fraction is 85(14)% for the $4^+_{K=4} \rightarrow 4^+_{K=0}\gamma$ decay, satisfying both the present γ-ray yield data and the previous measurement of 82(10)% $E2$ [41].

4. The 6+ isomer band at 1554 keV

The gyromagnetic ratio for a state of spin I is given by [7]

$$g(I) = g_R + (g_K - g_R)\frac{K^2}{I(I+1)}, \tag{2}$$

where g_K and g_R are characteristic of the single-particle and rotational motions, respectively. (The two factors g_K and g_R are independent to a first approximation, but are not completely

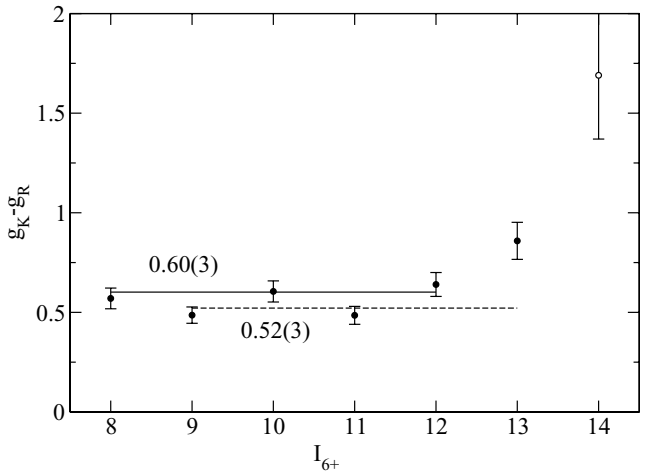

FIG. 31. The $g_K - g_R$ measurements for the $K = 6^+$ isomer band. The deviant point at spin 14^+ is thought to be the result of a doublet between the $15^+ \rightarrow 14^+$ and $14^+ \rightarrow 13^+\gamma$ decays. The solid and dashed lines are fits to the even ($I < 14$) and odd points, respectively.

decoupled [56].) If the gyromagnetic moments $\mu_1 = g_1 I$ and $\mu_2 = g_2 I$ are known for two particles or quasiparticles, the net moment can be calculated according to the additivity relation [57],

$$g(I) = \frac{1}{2}(g_1 - g_2) + \frac{j_1(j_1+1) - j_2(j_2+1)}{2I(I+1)}(g_1 - g_2), \quad (3)$$

for two particles with angular momenta j_1 and j_2 in a state of total angular momentum I.

In-band intensity ratios $\Gamma_{\Delta I=2}/\Gamma_{\Delta I=1}$ measured in the Xe beam experiment were used to determine the value of $g_K - g_R$, giving a mean value for the $8^+_{K=6}$–$13^+_{K=6}$ states (Fig. 31) of $g_K - g_R = 0.56(2)$. The value $g_R = 0.48(2)$ was obtained using Eq. (2) and a previous measurement of $g = 0.959(8)$ [58] for the 6^+ state. This leads to a value of $\bar{g}_K = 1.04(3)$ for the 6^+ band, in agreement with Mullins' measurement of 1.06(7) [32], calculated using the same g measurement.

Khoo has proposed a $69\%\pi\frac{7}{2}^+[404], \pi\frac{5}{2}^+[402]$ plus $31\%\nu\frac{7}{2}^-[514], \nu\frac{5}{2}^-[512]$ structure for the 6^+ band [44]. The expected values of $g_K^{\nu^2}$ and $g_K^{\pi^2}$ are 0.222 and 0.768, respectively, using Eq. (3) and measured values of the single-particle contributions from even-odd neighbors [59–61]. The 31% ν^2 component seems unlikely, because the present value of $\bar{g}_K$ is not in agreement with a ν^2 admixture, and the $\frac{5}{2}^-[512]$ Nilsson orbital should be occupied in the ground state. It could be argued that there may be other proton admixtures (e.g., the next $\frac{5}{2}^+[642]$ orbital in the $f_{7/2}$ subshell) that could contribute to a large value of g_K, but this $f_{7/2}$ orbital, combined with the $g_{7/2}$ proton, would be expected to give $\bar{g}_K = 0.84$. No other two-proton Nilsson state appears to have the correct parity, K value, and band head energy for the 6^+ state. The present measurement agrees with Mullins' conclusion that the 6^+ band is purely or predominantly π^2 in character.

The precise measurements of $B(\mathcal{M}\lambda)$ values of the 6^+ isomer decay branches, combined with the Alaga rule (for K-allowed transitions) and the SDM model (for K-forbidden transitions) yielded a strikingly accurate reproduction of the 6^+ isomer band Coulomb excitation yields with no adjustable parameters. Within the confines of the Alaga and SDM systematics, the intrinsic matrix elements coupling the $K^\pi = 0^+, 2^+, 4^+$, and 6^+ bands were derived from the measured $B(\mathcal{M}\lambda)$ values (Table IV).

The correct choice of relative phases of $\langle 6^+|E2|\gamma\rangle$ and $\langle 6^+|E2|4^+\rangle$ was more apparent than the analogous problem in the 4^+ band. Because the $\langle 6^+|E2|\mathrm{GSB}\rangle$ matrix element is much less effective than the other two, the problem could be treated as a two-path interference problem, showing that the only effective choice of phases is that of constructive interference between $\langle 6^+|E2|\gamma\rangle$ and $\langle 6^+|E2|4^+\rangle$ (Figs. 25 and 26). At large θ_{scat} angles, the $\langle 6^+|E2|\mathrm{GSB}\rangle$ term becomes more important. The overprediction of the yields for large $\theta_{\mathrm{scat}} > \theta^{\mathrm{safe}}_{\mathrm{scat}}$ can be explained by two conclusions: (1) The SDM model overpredicts $B(E2)$ strengths at high spin or (2) Coulomb-nuclear interference is becoming important above the $\theta^{\mathrm{lab}}_{\mathrm{scat}} = 53^\circ$ safe angle. The decreased success of the SDM model for higher-K bands indicates the former.

Coulomb excitation calculations, using the final set of matrix elements, indicate that the $I \rightarrow I + 2$ excitations are most effective in populating the 6^+ band and that the excitation generally follows the path of the fewest possible steps. The three paths to the excitation of the 6^+ band are illustrated in Fig. 18.

5. The 8^- isomer band at 1147 keV

The intrinsic quadrupole moment of the 8^- band could not be determined from the intraband γ-ray yields, because of the high sensitivity of the calculated yields to the inter-band $E3$ matrix elements. The authors of Refs. [32,56,62] have used the value $eQ_0 = 6.95$ eb ($\sqrt{\frac{5}{16\pi}}eQ_0 = 2.19$ eb), apparently originating from an early measurement of the $B(E2; 2^+_{K=0} \rightarrow 0^+_{K=0})$ strength [56], but direct measurements of the quadrupole moment of the 8^- isomer band have not been made. Measurements for the 16^+ isomer state of $Q_0 = 7.2(1)$b [63] and $Q_0 = 8.2(11)$ b [64] suggest that the 8^- bands would have very similar quadrupole moments to both the 16^+ band and the GSB, because the 16^+ isomer is believed to be the product of the two-quasiparticle wave functions of the two 8^- bands.

The present analysis of the 8^- isomer band population has shown that the coupling (and therefore the mixing) between the two 8^- bands is important in reproducing the Coulomb excitation yields of both bands. Previous experiments have led to measurements of the mixing amplitudes between the 8^-_1 and 8^-_2 bands [32,47,56,62,65,66]. Most results indicate that the 8^-_1 (isomer) band is predominantly a ν^2 band and that mixing is strong, with interaction potentials of $\gtrsim$100 keV. The present and past measurements of the mixing of the 8^- bands can be understood in terms of simple two-state mixing [67]. The mixed-state (perturbed) wave functions ψ_A and ψ_B can be written in terms of the unperturbed (pure) basis states ϕ_a and ϕ_b as

$$\begin{aligned} \psi_A &= \alpha\phi_a + \beta\phi_b \\ \psi_B &= -\beta\phi_a + \alpha\phi_b, \end{aligned} \quad (4)$$

where $\alpha^2 + \beta^2 = 1$. The interaction potential V between the unperturbed states is defined as

$$V = \langle \phi_a | \hat{V} | \phi_b \rangle \tag{5}$$

or

$$V = \frac{\Delta E_f}{\sqrt{\frac{x^2}{1+x} + 4}} \tag{6}$$

in terms of the measured separation energy ΔE_f between the mixed states and the mixing fraction β^2 [68], where $x \equiv \frac{1}{\beta^2} - 2$. The observed gyromagnetic ratios $\bar{g}_K$ of the mixed states are given by

$$\bar{g}_K^A = (1-\beta^2) g_K^a + \beta^2 g_K^b$$

and

$$\bar{g}_K^B = \beta^2 g_K^a + (1-\beta^2) g_K^b, \tag{7}$$

where g_K^a and g_K^b are the gyromagnetic ratios of the unperturbed basis states. Then, for the $8_1^- – 8_2^-$ system, composed as $\psi_{8_1^-} = \alpha \phi^{\nu^2} + \beta \phi^{\pi^2}$, the observed gyromagnetic ratio $\bar{g}_K = (1-\beta^2) g_K^{\nu^2} + \beta^2 g_K^{\pi^2}$ can be used to measure β^2. For any two-state mixing system an interaction energy of $V \approx \frac{\Delta E_f}{2}$ (166 keV for the 8_1^- and 8_2^- system) indicates that two nearly degenerate basis states are almost completely mixed.

Helmer and Reich [65] proposed that the 8_1^- isomer band is a mixed two-quasiproton ($\pi \frac{9}{2}^-[514] \pi \frac{7}{2}^+[404]$) and two-quasineutron ($\nu \frac{7}{2}^-[514] \nu \frac{9}{2}^+[624]$) configuration, approximately one third π^2 from their measured γ-ray intensities. This proposed $\pi \frac{9}{2} \pi \frac{7}{2}$, $\nu \frac{7}{2} \nu \frac{9}{2}$ configuration is also consistent with succeeding measurements of the gyromagnetic moments.

Two intraband branching ratios were measured in the Hf(Xe, Xe)Hf data for the 11^- and 10^- levels. Assuming the same quadrupole moment as in the GSB, the branching ratios yield $|g_K - g_R| = 0.12(7)$ for the 11^- state. (The branching ratio of the 10^- state does not give a real solution for $g_K - g_R$, and Eqs. (7) imply that the $10^- \rightarrow 9^-$ decay is $\approx$100% $E2$, but the measured γ-ray intensity ratio was $I_\gamma^{\Delta I=2} / I_\gamma^{\Delta I=1} = 2.2(3)$, compared to previous measurements of 1.67(10) [42] and 1.8(5) [47].)

Using $g_R = 0.48(2)$ from the present 6^+ band measurements and previous calculated g_K values [56] for the neutron and proton configurations of the 8^- band, the present measurements of branching ratios for the 11^- state indicate a 58(7)% π^2 component, about twice the result of Tlustý *et al.* [62] (Fig. 32, bottom panel). However, V differs by at most 15% from previous measurements [Fig. 32 (top), error from the branching ratio]. For $g_R \approx 0.3$ (a commonly assumed value for ^{178}Hf, which can be obtained from an unweighted average of experimental g_R values for the quasiparticle configurations of the two 8^- states [69]), the present data would give a 41(6)% π^2 component in the 8_1^- band.

Table VIII gives π^2 admixture fractions in the 8_1^- states (β^2) and their corresponding interaction potentials V from previous and present measurements. In contrast, in lighter isotopes (e.g., ^{172}Hf [58], ^{174}Hf [70], ^{176}Hf [71]) the configuration of the lower of the two 8^- band heads (the only one observed in ^{172}Hf) has been identified as a nearly pure π^2 state, whereas

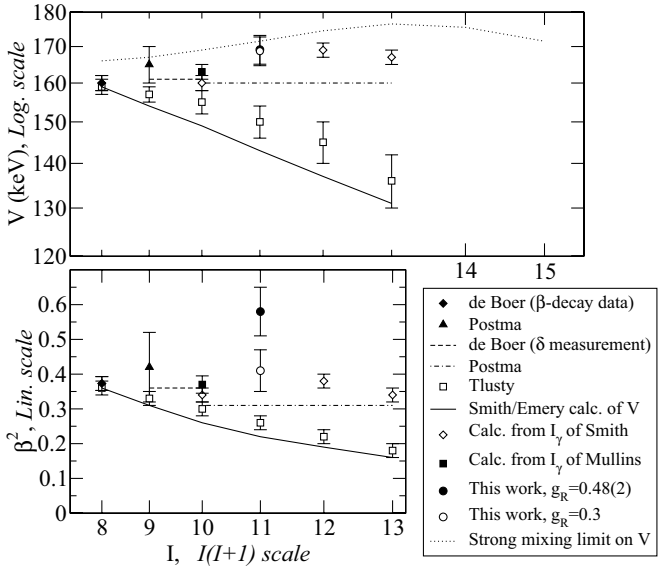

FIG. 32. Measured and calculated values of β^2 (bottom) and V (top) values, as a function of $I_{8_1^-}$. For strong mixing, large fractional variations in β^2 result in small fractional variations in V.

all previous measurements for ^{178}Hf indicate a strongly mixed system, with a dominant ν^2 admixture in the isomer band. However, the energies of the 8^- isomers in the lighter isotopes are 400–850 keV higher than ^{178m}Hf, so that a difference might be expected in the strength of the mixing of the 8^- states in ^{178}Hf.

The proton contributions to $\bar{g}_K$ are dominant, and with $g_R \approx 0.3$ for ^{178}Hf, a maximum 70% ν^2 component is predicted in the limit $g_K - g_R \rightarrow 0$, using the values $g_K = 1.031(11)$ for the $\pi \frac{9}{2}^- \pi \frac{7}{2}^+$ state and $g_K = -0.013(3)$ for the $\nu \frac{7}{2}^- \nu \frac{9}{2}^+$ state [56]. Naturally, measurements of relative intensities that would give $(g_K - g_R)^2 < 0$ after subtraction of the $E2$ component give no meaningful result, so that for estimates of $g_R \approx 0.3$, the lower bound on measurements of the π^2 fraction is 30%, not far from many published measurements (Table VIII and Figure 32). However, the mixing potential V varies slowly with β^2 for strongly mixed states, such as in the present case, and can be measured to good precision within the two-state mixing model. (For the two mixed $8_{K=8}^-$ states separated by $\Delta E = 332$ keV, $0.25 \leqslant \beta^2 \leqslant 0.35 \Rightarrow 144 \leqslant V \leqslant 158$ keV.)

6. *The* 14^- *isomer band at 2574 keV*

It was not possible to find an unambiguous indication of population of the 14^- isomer band, but an upper limit on the cross section was calculated from the γ-ray doubles data. A $\langle K = 14 | E3 | K = 0 \rangle$ matrix element was fit to the upper limit, assuming that the 14^- band is populated directly from the GSB by matrix elements $\langle I_f, K = 14 \| E3 \| I_i, K = 0 \rangle \approx 1.3$ eb$^{3/2}$, all of approximately equal magnitude. The upper limit on the isomer cross section was calculated for the Xe beam experiment based on this simple model, giving $\sigma_{14^-} <$ 2 mb, considerably smaller than those of the other isomers populated in this work (Table VII).

TABLE VIII. A survey of measurements of V and β^2 values of the 8_1^- band states. Errors in V were calculated from the errors in the authors' measured quantities. Systematic uncertainties in estimates of g_R and g_K values are not included.

I	$g_K - g_R$ (or δ)	β^2	V (keV)	$\frac{V}{E_{8_2^-}(I)-E_{8_1^-}(I)}$
8–13		≈0.4	(Ref. [65]) ≈167	≈0.49
8		0.373(20)[a]	(Ref. [56]) 160(2)	0.484(5)
8		0.36(2)[b]	(Ref. [62]) 159(2)	0.480(6)
8		0.36[c]	(Ref. [47]) 159[c]	0.479
9–10	0.096(9),0.103(17)	0.360(16)[d]	(Ref. [56]) 160(2)–162(2)	0.480(5)
9	($0.64 \leqslant \delta \leqslant 1.88$)	0.42(10)[e]	(Ref. [66]) 165(5)	0.494(16)
9	0.097(12)	0.33(2)[b]	(Ref. [62]) 157(2)	0.470(7)
9		0.31[c]	(Ref. [47])154[c]	0.461
10–13		0.31(3)[f]	(Ref. [66,79]) 156(4)–163(4)	0.462(12)
10	0.099(18)	0.30(2)[b]	(Ref. [62]) 155(3)	0.458(9)
10		0.370(25)[g]	(Ref. [42]) 163(2)	0.483(7)
10		0.34(2)[h]	(Ref. [47]) 160(2)	0.474(7)
10		0.26[c]	(Ref. [47]) 149[c]	0.441
11	0.036(13)	0.26(2)[b]	(Ref. [62]) 150(4)	0.439(11)
11		0.22[c]	(Ref. [47]) 143[c]	0.417
11	0.12(7)	0.58(7)[i]	169(4)	0.494(11)
12	0.00(12)	0.22(2)[b]	(Ref. [62]) 145(5)	0.414(14)
12		0.38(2)[h]	(Ref. [47]) 169(2)	0.485(5)
12		0.19[c]	(Ref. [47]) 137[c]	0.393
13	−0.039(18)	0.18(2)[b]	(Ref. [62]) 136(6)	0.384(17)
13		0.34(2)[h]	(Ref. [47]) 167(2)	0.474(7)
13		0.16[c]	(Ref. [47]) 131[c]	0.371

[a]From β-decay experiments.
[b]From a simultaneous fit of $g_K - g_R$ to a quadratic function of $\vec{I}^2$. The author's largest error estimate was used.
[c]V calculated in Ref. [47], β^2 calculated from V.
[d]Reference [56] used $g_R = 0.262(14)$.
[e]From δ, using $g_K - g_R$ from Ref. [56].
[f]Calculated in Ref. [66] from the data of Ref. [79].
[g]Calculated from the intraband intensity ratios of Ref. [42] using $g_R = 0.3$.
[h]Calculated from the intraband intensity ratios of Ref. [47] using $g_R = 0.3$.
[i]Present work.

7. *The* 16^+ *isomer band at 2446 keV*

The 16^+ band appears to be populated directly from the GSB (Fig. 18). In the Xe beam experiment, Coulomb excitation calculations based on the fitted matrix elements showed that the principle mode is by γ-decay feeding from the GSB (≈10% by direct excitation). The $E2$ strength deduced from the combined data of the Xe-beam and Ta-target experiments is $\leqslant$1.4 W.u. (Table VI), and the modest 0.05–0.14 W.u. transitions to the 16^+ and 17^+ states are responsible for ≈80% of the isomer population in the Xe experiment, as a consequence of the high energies of the γ-ray feeding transitions. The measured (model-independent) 16^+ isomer cross sections from the ^{178}Hf beam activation experiment (Table VII) gave an excitation probability of $14(5) \times 10^{-4}$ at 80% of the Coulomb barrier, whereas the isomer excitation probability for the $25^\circ \leqslant \theta_{\rm scat}^{\rm lab} \leqslant 78^\circ$ scattering range in the ^{136}Xe beam experiment was $4(2) \times 10^{-4}$ (calculated from the fitted matrix elements).

A direct measurement of the quadrupole moment of the 16^+ band using laser spectroscopy on ^{178m2}Hf nuclei gave $Q_0 = 7.2(1)$ b [63], whereas Coulomb excitation of a 16^+ isomer-enriched target gave $Q_0 = 8.2(11)$ b [64]. The first measurement is within 5% of the Q_0 moment of the GSB, and the second is within ≈1σ (19% greater), but the $19^+ \rightarrow 18^+$ yields were not sensitive enough to the quadrupole moment to allow a measurement using the present data sets.

B. *K* mixing

The sets of EM reduced matrix elements for K-forbidden transitions to the high-K bands, or, equivalently, the hindrance values for the transitions, reveal the systematics of K mixing and identify the bands where the mixing occurs. Decreasing hindrance of the transitions between two bands can be understood in terms of increasing K mixing in the wave functions of one or both bands.

Reduced hindrance values range from $f_\nu = 9.6$ to 23 for the K-forbidden $E2$ decay branches of the 4^+ band head to the GSB and the γ-band—within the limits set by the measured bounds on the lifetime, but well below the value of 100 of the Rusinov rule frequently suggested for K-forbidden transitions [21,72]. The GSB$\rightarrow$ $K = 4^+$ coupling of the SDM model fit

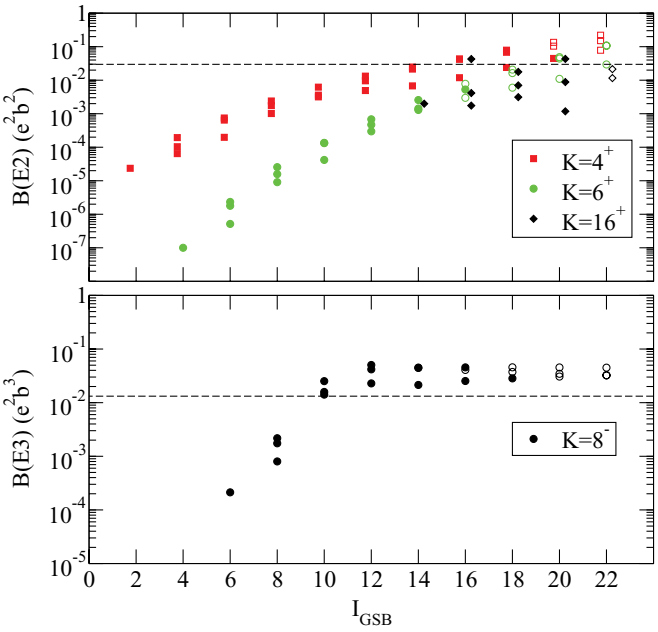

FIG. 33. (Color online) The three strongest reduced transition probabilities from each GSB level for GSB$\rightarrow$ K^π transitions. GSB$\rightarrow$ $4^+, 6^+$ matrix elements follow the SDM model. GSB$\rightarrow$ 8^- matrix elements follow the Alaga rule, attenuated at low spin. Transitions to unobserved high-spin levels (hollow), are extrapolated to clarify the spin dependence of the intrinsic matrix elements in the models used. Weisskopf estimates (dashed lines): $B(E2\uparrow)_{\rm W} = 0.0297\ {\rm e^2b^2}$. $B(E3\uparrow)_{\rm W} = 0.0132\ {\rm e^2b^3}$.

predicts lower reduced hindrance values above the band head ranging from 9.0 to 4.9 for the stretched $E2$ $K = 4 \rightarrow$ GSB transitions from the $I^\pi_{K=4} = 6^+$ to 18^+ states.

The 6^+ band yields were reproduced by K-forbidden transitions from the GSB with f_ν decreasing from 24 to 5 for the $\Delta I = +2$ electric quadrupole transitions from the $I_{\rm GSB} = 4$ to the $I_{\rm GSB} = 12$ state. Similarly, from the $I_\gamma = 4$ state to the $I_\gamma = 10$ state, the γ-band$\rightarrow$ $K = 6$ reduced hindrance decreased from 14 to 3, for $\Delta I = +2$ transitions.

The present analysis of the $K^\pi = 8^-$ band Coulomb excitation data from the Hf(Xe, Xe)Hf experiment [4] led to a set of matrix elements populating the 8^- bands, which were attenuated by approximately an order of magnitude per unit of spin as $I_{\rm GSB}$ decreased from $10\hbar$ to $6\hbar$ (Fig. 33). This attenuation was required to keep the isomer cross section from growing unreasonably large compared to the other isomers and to preserve the 4.0(2) s half-life, while simultaneously reproducing the measured γ-ray yields. A similar attenuation was required in the γ-band$\rightarrow$ $K^\pi = 8^-$ matrix elements (Fig. 34 and Table IX). The gradual increase in strength of the $B(E3)$ with increasing I_γ or $I_{\rm GSB}$ resulted in a drop in the reduced hindrance from $f_\nu = 2.3$ to 0.9 for the $\Delta I = +3$ excitations from the 6^+ to 12^+ levels.

The GSB$\rightarrow$ $K^\pi = 16^+$ matrix elements deduced from the combined data of the isomer activation experiment and the prompt $19^+ \rightarrow 18^+ \gamma$-ray yields of the Xe beam experiment are comparatively constant with increasing spin, in contrast with the K-forbidden matrix elements populating the $K^\pi =$ $4^+, 6^+$, and 8^- bands. The intrinsic matrix element and the $B(E2; {\rm GSB} \rightarrow K = 16)$ values are nearly saturated at $\sim$1 W.u. (the approximate upper bound expected for noncollective transitions) by $I_{\rm GSB} = 14$, the lowest GSB state that populates the isomer band. Hence, there is no hindrance of the GSB$\rightarrow$ $K = 16$ transitions due to K forbiddenness at $I_{\rm GSB} = 14$. In contrast, the K-forbidden matrix elements populating the $K = 4$–8 bands take values $\geqslant$4 orders of magnitude below their saturation values at the lowest $I_{\rm GSB}$ and I_γ connections (Figs. 33 and 34). Even with transition probabilities $<0.1\ {\rm e^2b^2}$ feeding the 16^+ band, the reduced hindrance values f_ν range from 0.87 to 1.10, a factor of 100 smaller than the prediction of Rusinov's rule.

The $16^+_{\rm isom} \rightarrow K^\pi = 8^-$ and $14^-_{\rm isom} \rightarrow K^\pi = 8^-$ decays are all highly hindered [34,47], showing that the onset of significant high-K admixtures does not occur at sufficiently low spin ($I^\pi = 12^-, 13^-$) in the 8^- band to account for the observed 8^- isomer band yields. Hence, mixing in the high-K bands is unable to explain the Coulomb excitation of all of the high-K bands, whereas the measured matrix elements are consistent with increasing mixing in the low-K bands in every instance.

The systematic decrease with increasing spin of the hindrance of K-forbidden transitions is apparent from Figs. 33 and 34 and Table IX. For each of the high-K isomer bands observed, reproduction of the measured yields requires that the interband $B(E\lambda)$ values increase with increasing spin and saturate at $\approx$1 W.u. for $I \gtrapprox 12$ in the GSB and the γ band. This saturation point represents the maximum mixing

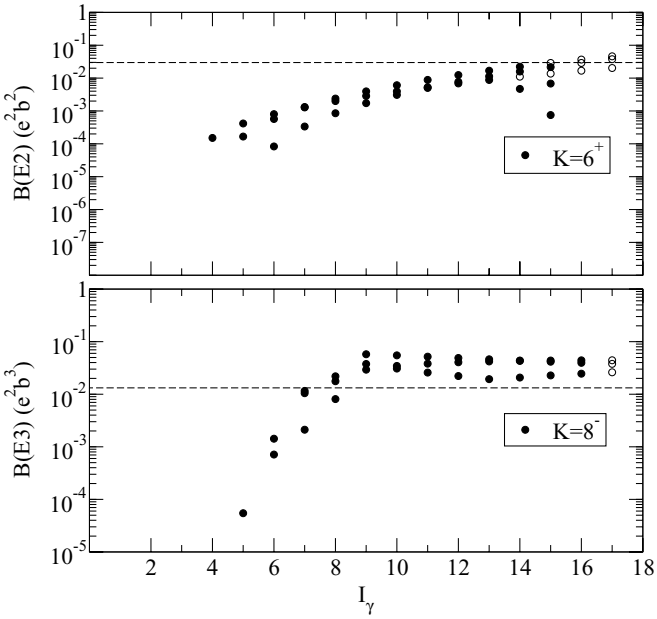

FIG. 34. The three strongest reduced transition probabilities from each γ-band level for γ-band$\rightarrow$ K^π transitions. The γ-band$\rightarrow$ 6^+ matrix elements follow the SDM model. The γ-band$\rightarrow$ 8^- matrix elements follow the Alaga rule, attenuated at low spin. Transitions to unobserved high-spin levels (hollow), are extrapolated to clarify the spin-dependence of the intrinsic matrix elements in the models used. Weisskopf estimates (dashed lines): $B(E2\uparrow)_{\rm W} = 0.0297\ {\rm e^2b^2}$. $B(E3\uparrow)_{\rm W} = 0.0132\ {\rm e^2b^3}$.

TABLE IX. Values of the reduced hindrance f_ν given in the direction $I_i \to I_f$ for selected K-forbidden transitions in ^{178}Hf. Weisskopf estimates $B(\mathcal{M}\lambda\downarrow)_{\text{W.u.}}$ are 0.020 e^2b ($E1$), 6.0×10^{-3} e^2b^2 ($E2$), 2.0×10^{-3} e^2b^3 ($E3$), 2.2×10^{-4} e^2b^5 ($E5$), 1.8 μ_N^2 ($M1$), 0.52 $\mu_N^2 b$ ($M2$), 0.055 $\mu_N^2 b^3$ ($M4$). Defined $B(\mathcal{M}\lambda\uparrow)_{\text{W.u.}} \equiv (2\lambda+1)B(\mathcal{M}\lambda\downarrow)_{\text{W.u.}}$.

Bands	I_i	I_f	$\mathcal{M}\lambda$	ν	f_ν
GSB $\to K^\pi = 4^+$	2	4	$E2$	2	35.
	6	8	$E2$	2	12.
	12	14	$E2$	2	18.
GSB $\to K^\pi = 6^+$	4	6	$E2$	4	24.
	8	10	$E2$	4	8.
	12	14	$E2$	4	5.
GSB $\to K^\pi = 8^-$	8	8	$E1$	7	67(1)[a]
	6	8	$M2$	6	>130[a]
	8	11	$E3$	5	1.5
	10	13	$E3$	5	1.0
	12	15	$E3$	5	0.9
GSB $\to K^\pi = 16^+$	12	16	$E4$	12	>9[a]
	14	16	$E2$	14	1.2
	16	18	$E2$	14	1.0
	18	20	$E2$	14	1.0
	20	21	$E2$	14	1.0
$K^\pi = 2^+ \to K^\pi = 6^+$	4	6	$E2$	2	14.
	6	8	$E2$	2	6.
	8	10	$E2$	2	3.9
	10	12	$E2$	2	2.7
$K^\pi = 2^+ \to K^\pi = 8^-$	5	8	$E3$	3	6.
	7	10	$E3$	3	1.0
	9	12	$E3$	3	0.7
	11	14	$E3$	3	0.8
$K^\pi = 16^+ \to K^\pi = 8^-$	16	11	$E5$	3	165(5)[b]
(isomer decays)	16	12	$M4$	4	72(2)[b]
	16	13	$E3$	5	66(1)[b]
$K^\pi = 14^- \to K^\pi = 8^-$	14	13	$M1$	5	90[c]
(isomer decays)	14	12	$E2$	4	33[c]

[a]Calculated from Ref. [47].
[b]Reference [47].
[c]Reference [34].

of K. For $I \geqslant 12$, reduced hindrance values of K-forbidden transitions from low-K to high-K bands are as low as $f_\nu \sim 1$, indicating that for these transitions the K-selection rule has little predictive power at high spin, i.e., highly K-forbidden transitions have strengths similar to allowed interband transitions. A notable exception is the unobserved $12^+_{\text{GSB}} \xrightarrow{E4} 16^+_{\text{K=16}}$ excitation whose hindrance (Table IX) suggests that the $K = 12$ admixture in the GSB is insignificant for $I < 14$. The $8^+_{\text{GSB}} \xrightarrow{E3} 8^-_{\text{K=8}}$ ($f_\nu > 9$) and $6^+_{\text{GSB}} \xrightarrow{E3} 8^-_{\text{K=8}}$ ($f_\nu > 70$) transitions [73] suggest that the Alaga rule may not describe well all of the K-forbidden couplings. Compared to the Alaga rule, a more rapid increase in the magnitudes of the EM matrix elements was found in the low-K to $K \leqslant 8$ transitions.

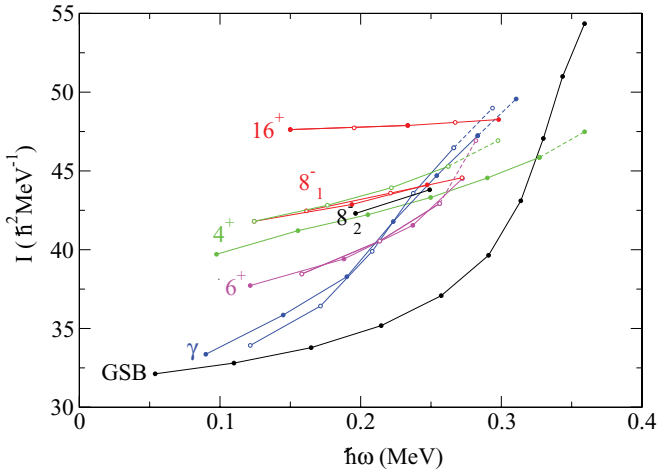

FIG. 35. (Color online) Measured moments of inertia of ^{178}Hf rotational bands. Dashed lines connect to tentatively assigned levels. The first transition in each trace is the $I_i = K+2 \to I_f = K$ transition. The 16^+ band data are from Mullins *et al.* [32].

Band interactions are reflected in the measured moments of inertia by an increase in slope of the moment of inertia $I(\omega)$, seen at $I \approx 6$ and $I \approx 10$ in the γ and GS bands, respectively (Fig. 35). As described in Sec. IV D, the $B(E\lambda)$ values saturate at ~1 W.u. as low as $I \approx 8$ and $I \approx 10$ for transitions from the γ-band and the GSB, respectively, to reproduce the measured γ-ray yields in the $K^\pi = 4^+, 6^+, 8^-$, and 16^+ bands. Moreover, Coriolis alignment is expected to happen at much lower spin in low-K bands than in high-K bands [74], which are strongly deformation coupled. The moments of inertia of the high-K bands are relatively constant in slope, with the exception of the 6^+ band at $I \approx 12$, consistent with purity of the high-K bands up to much higher spin, compared to the low-K bands. The 16^+ band has a remarkably constant moment of inertia [32] up to $I = 22$, consistent with, but not necessarily indicative of, the nearly constant $B(E2; \text{GSB} \to K = 16)$ values with $f_\nu \approx 1$. (Mixing in high-K bands can also produce a fairly constant moment of inertia [75].)

The $16^+_{\text{isom}} \to K^\pi = 8^-$ and $14^-_{\text{isom}} \to K^\pi = 8^-\gamma$ decays are strongly hindered with $33 \leqslant f_\nu \leqslant 165(5)$ in all of the five known branches, indicating that the onset of significant high-K admixtures in the 8^- band must occur at $I > 13$, if at all, whereas less hindered $f_\nu \sim 1$ transitions from the γ and GS bands are required to reproduce the present measured yields. That is, the strongly hindered decays of the 16^+ and 14^- isomers to the $11^- \leqslant I^\pi_{K=8} \leqslant 13^-$ states are consistent with K being a good quantum number for the high-K bands, suggesting that mixing in the low-K bands is primarily responsible for the K-selection violations and that the EM matrix elements coupling to the high-K bands are sensitive probes of the K distributions in the low-K bands. Coulomb excitation of a band with projection K, assuming that it is reasonably pure, would require admixtures K' in the low-K (nominally K_i) bands of $K-\lambda \leqslant K' \leqslant K+\lambda$. Hence, the mixing fractions of the $2 \leqslant K' \leqslant 6$ components are depicted in Figs. 33 and 34 as a function of spin by the

$B(E2; K_i \rightarrow K = 4)$ values, the $4 \leqslant K' \leqslant 8$ components by the $B(E2; K_i \rightarrow K = 6)$ values, the $5 \leqslant K' \leqslant 11$ components by the $B(E3; K_i \rightarrow K = 8)$ values, and the $14 \leqslant K' \leqslant 18$ components by the $B(E2; K_i \rightarrow K = 16)$ values. In the absence of any contradictory information, it might be assumed that the lowest K value in each range enters the wave function first. Hence, the EM matrix elements coupling to the high-K bands are sensitive probes of the K distributions in the low-K bands.

Two effects have been postulated to explain the mixing of high- and low-K states: alignment of the single-particle or quasiparticle angular momenta due to collective rotations, and triaxial deformation effects such as softness to γ deformation and γ-barrier tunneling. The γ-barrier penetration hypothesis has had success in explaining K violations in more γ-soft nuclei such as ^{182}W and ^{181,182,184}Os. However, the same treatment does not reproduce the measured hindrance values in more γ-rigid Hf nuclei [13,16]. The γ-barrier penetration calculations make an absolute prediction of K-forbidden transition probabilities, but do not make predictions above the band head, high in the rotational bands where the present work predicts significant transition probabilities. K mixing in the band head is a necessary feature of the γ-tunneling hypothesis, but this is strongly disputed by the high measured hindrance values of isomer decay branches. Predictions by Narimatsu *et al.* [13] of the hindrance of isomer decay branches are in agreement with measured hindrance values for γ-soft nuclei but differ by several orders of magnitude in the Hf nuclei, ^{178}Hf for instance.

The present work has resulted in measurements that are qualitatively similar to the SDM model in the most deviant cases (8^-, 16^+)—a rapid increase in mixing with increasing spin and a pure high-K band head—and agree quantitatively with the SDM model (with two adjustable parameters) in the $K \leqslant 6$ data. In the case of the $K^\pi = 8^-$ band, the sets of matrix elements derived from the data qualitatively follow the decrease in hindrance with increasing spin predicted by the SDM model and are consistent with the Coriolis mixing hypothesis. Perhaps, with higher-order corrections, the SDM model would be useful for higher-K bands.

The predictions of the projected shell model (PSM) are not limited to the high-K band heads or to very small rotations R as is the case in the γ-tunneling models. Rather, a softness to γ deformations is predicted in ^{178}Hf for all states, including low-lying GSB states [17]. This would naturally lead to K mixing in all bands with the loss of axial symmetry for $\gamma > 0$. The PSM in its current state of development gives good agreement with some isomer level energies, but it has not yet been used to calculate EM transition matrix elements. The predicted γ softness is not in conflict with the Coriolis mixing model, and future calculations may show that γ softness makes an additional contribution to the measured strength of K-forbidden transitions to the isomer bands.

Neither of these two models has made absolute predictions of a complete set of K-forbidden matrix elements. Nor does γ-barrier tunneling [1,76] make quantitative predictions above the isomer band head. The present experimental probe of the loss of K conservation and the measured decrease in the hindrance of K-forbidden transitions with increasing spin in the low-K bands demonstrates the need for further theoretical work.

C. Coulomb depopulation

Based on the present measurements of the $\langle K^\pi = 16^+ \| E2 \| \mathrm{GSB} \rangle$ matrix elements, the $16^+ \stackrel{E2}{\rightarrow}$ GSB K-forbidden paths would allow Coulomb depopulation of the $K^\pi = 16^+$, 31-yr isomer using heavy ions, resulting in a cascade of 93- to 718-keV γ rays and a net energy gain of 2.4 MeV. Calculations for a 230 MeV ^{58}Ni beam on a thin $\sim$1-mg/cm^2 isomeric target predict a depopulation probability of $\leqslant$1% [77] compared to the in-band excitations. The known strength of the K-allowed $M2$ decay of the 14^- isomer to the 16^+ isomer (Fig. 28) is irrelevant in Coulomb excitation, but the allowed $E3$ transitions would have a $\lesssim$1% probability [77] assuming typical $E3$ matrix elements in ^{178}Hf, whereas $\approx$50% of the 14^- excitation would decay back to the 16^+ isomer. Neither of these paths would be effective for photodeexcitation of the isomer, because photon absorption is dominated by $E1$ transitions, but this does not rule out depopulation via a K-forbidden ($\nu = 1$) 463-keV $E1$ photoexcitation to the 15^-_{14} state, for example. The $16^+ \stackrel{E3}{\rightarrow} 8^-$ transitions are highly forbidden because K is well-defined in the high-K bands, as it has been shown above, making this path ineffective. Although low-yield Coulomb deexcitation paths have been discovered, intermediate states that might mediate the reported stimulated emission of the $K^\pi = 16^+$ isomer [78] were not found.

VI. CONCLUSION

A ^{178}Hf(^{136}Xe,^{136}Xe)^{178}Hf experiment using CHICO [23] and Gammasphere [24] demonstrated substantial K-forbidden Coulomb excitation of the $K^\pi = 4^+$ rotational band, as well as the rotational bands built on the $K^\pi = 6^+$ and 8^- isomers. Several rotational bands in ^{178}Hf were extended from the previously known states to spin $15\hbar$–$18\hbar$. Remarkably, the $K^\pi = 16^+$ isomer band in ^{178}Hf was populated by Coulomb excitation with nearly the same strength as the $K^\pi = 6^+, 8^-$ isomer bands, despite the $\nu = 14$ forbiddenness. Data from Coulomb excitation of the $K^\pi = 16^+$ isomer via Ta(^{178}Hf,^{178}Hf)Ta beam excitation provided an unambiguous indication that the isomer was populated by *safe* Coulomb excitation with collision energies as low as 73% of the Coulomb barrier and confirmed the remarkably high population of the 16^+ isomer band in the former experiment.

A set of model-dependent intrinsic matrix elements was measured, which couple the $K^\pi = 0^+, 2^+, 4^+, 6^+$, and 8^- bands in ^{178}Hf. The $K^\pi = 16^+$ isomer band was found to be populated directly from the GSB, and upper and lower bounds on a consistent set of $\langle I_{K=16} \| E2 \| I_{K=0} \rangle$ matrix elements were determined. The deduced matrix elements provided the first qualitative measurement of the K distribution with respect to nuclear spin in low-K bands and revealed the rapid breakdown of the goodness of the K quantum number as the low-K bands are excited to higher rotational frequencies. The rapid increase in the interband $E\lambda$ matrix elements coincides with

the rotational alignment of low-K bands that has a noticeable effect on the moment of inertia above the $I \approx 10$ levels of the γ band and the GSB. Higher-K components are admixed in the nominally low-K bands with increasing spin, until the reduced transition probabilities saturate near $\sim$1 W.u. for $I \gtrapprox 12\hbar$ signifying the total breakdown of the K quantum number. The high-K bands remain quite pure, even at the same spin (I) levels where mixing in the the low-K bands has saturated. The present measurements are consistent with Coriolis alignment.

Coulomb excitation probabilities were calculated for depopulation of nuclei in the 16^+ isomer state, based on the present set of $\langle I_{K^\pi=16^+} \| E2 \| I_{\mathrm{GSB}} \rangle$ matrix elements. Although a $\lesssim$1% Coulomb depopulation of the $K^\pi = 16^+$ isomer may be possible using heavy ions, no useful intermediate state was found that might mediate photodepopulation via $E1$ excitations.

The present work, initially focused on understanding the K-forbidden population of the $K^\pi = 8^-$ isomer in ^{178}Hf, has provided a variety of nuclear structure information. New levels and γ-ray information were used to probe physical properties of the $K^\pi = 0^+, 2^+, 4^+, 6^+, 8^-$, and 16^+ rotational bands, including K mixing. The observed breakdown of the K selection rule appears to be a result of collective rotational effects, so that the present conclusions regarding K mixing as a function of spin may offer an explanation of K-forbidden excitation and decay in other axially symmetric quadrupole-deformed nuclei.

ACKNOWLEDGMENTS

Work supported by the National Science Foundation and the Air Force Office of Scientific Research (Rochester); the U.S. Department of Energy grant W-7405-ENG-48 (LLNL), DE-FG02-91ER-40609 (WNSL) and contracts DE-FG02-05ER41379 and DE-FG52-NA25929 (Richmond), W-31-109ENG-38 (ANL), and DEAC03-76SF00098 (LBNL); and the Polish State Committee for Scientific Research contract 5P03B04720 (Warsaw). The graphic work of E. Subramanian is gratefully acknowledged.

[1] P. Chowdhury, B. Fabricius, C. Christensen, F. Azgui, S. Bjørnholm, J. Borggreen, A. Holm, J. Pedersen, G. Sletten, M. A. Bentley *et al.*, Nucl. Phys. **A485**, 136 (1988).
[2] P. M. Walker, G. Sletten, N. L. Gjørup, M. A. Bentley, J. Borggreen, B. Fabricius, A. Holm, D. Howe, J. Pedersen, J. W. Roberts *et al.*, Phys. Rev. Lett. **65**, 416 (1990).
[3] P. M. Walker, G. D. Dracoulis, and J. J. Carroll, Phys. Rev. C **64**, 061302(R) (2001).
[4] A. B. Hayes, D. Cline, C. Y. Wu, M. W. Simon, R. Teng, J. Gerl, C. Schlegel, H. J. Wollersheim, A. O. Macchiavelli, K. Vetter *et al.*, Phys. Rev. Lett. **89**, 242501 (2002).
[5] M. Loewe, P. Alexa, T. Czosnyka, J. de Boer, J. Iwanicki, A. I. Levon, H. J. Maier, P. J. Napiorkowski, P. von Neumann-Cosel, A. Richter *et al.*, Phys. Lett. **B551**, 71 (2003).
[6] A. B. Hayes, D. Cline, C. Y. Wu, J. Ai, H. Amro, C. Beausang, R. F. Casten, J. Gerl, A. A. Hecht, A. Heinz *et al.*, Phys. Rev. Lett. **96**, 042505 (2006).
[7] A. Bohr and B. R. Mottelson, *Nuclear Structure* (Benjamin, Reading, 1975), vol. 2.
[8] J. H. Hamilton, A. V. Ramayya, R. M. Ronningen, R. O. Sayer, H. Yamada, C. F. Maguire, P. Colombani, D. Ward, R. M. Diamond, F. S. Stephens *et al.*, Phys. Lett. **B112**, 327 (1982).
[9] H. Xie, C. Ender, J. Gerl, T. Härtlein, F. Köck, T. Kröll, P. Reiter, D. Schwalm, P. Thirolf, K. Vetter *et al.*, Phys. Rev. C **48**, 2517 (1993).
[10] P. M. Walker, D. M. Cullen, C. S. Purry, D. E. Appelbe, A. P. Byrne, G. D. Dracoulis, T. Kibédi, F. G. Kondev, I. Y. Lee, A. O. Macchiavelli *et al.*, Phys. Lett. **B408**, 42 (1997).
[11] P. Chowdhury (2005), presentation at the 12th International Conference on Capture Gamma-ray Spectroscopy and Related Topics.
[12] G. D. Dracoulis, F. G. Kondev, G. J. Lane, A. P. Byrne, T. Kibédi, I. Ahmad, M. P. Carpenter, S. J. Freeman, R. V. F. Janssens, N. J. Hammond *et al.*, in *Proceedings of the Conference on Nuclei at the Limits*, edited by D. Seweryniak and T. L. Khoo (American Institute of Physics, Melville, NY, 2005).
[13] K. Narimatsu, Y. R. Shimizu, and T. Shizuma, Nucl. Phys. **A601**, 69 (1996).
[14] S. K. Tandel, P. Chowdhury, E. H. Seabury, I. Ahmad, M. P. Carpenter, S. M. Fischer, R. V. F. Janssens, T. L. Khoo, T. Lauritsen, C. J. Lister *et al.*, Phys. Rev. C **73**, 044306 (2006).
[15] G. D. Dracoulis, G. J. Lane, F. G. Kondev, A. P. Byrne, T. Kibédi, H. Watanabe, I. Ahmad, M. P. Carpenter, S. J. Freeman, R. V. F. Janssens *et al.*, Phys. Rev. C **71**, 044326 (2005).
[16] T. R. Saitoh, N. Saitoh-Hashimoto, G. Sletten, R. A. Bark, G. B. Hagemann, and B. Herskind, Phys. Scripta T **88**, 67 (2000).
[17] Y. Sun, X.-R. Zhou, G.-L. Long, E.-G. Zhao, and P. M. Walker, Phys. Lett. **B589**, 83 (2004).
[18] S. Frauendorf, in *Proceedings of the International Conference on The Future of Nuclear Spectroscopy, Crete, Greece*, edited by C. A. Kalfas, W. Gelletly, S. Harissopulos, D. Loukas, and R. Vlastou, National Technical University Press, Athens (1993), p. 112.
[19] S. Frauendorf, Nucl. Phys. **A557**, 259c (1993).
[20] G. D. Dracoulis, F. G. Kondev, G. J. Lane, A. P. Byrne, T. R. McGoram, T. Kibédi, I. Ahmad, M. P. Carpenter, R. V. F. Janssens, T. Lauritsen *et al.*, Phys. Rev. Lett. **97**, 122501 (2006).
[21] L. I. Rusinov, Usp. Fiz. Nauk **73**, 615 (1961).
[22] F. G. Kondev, G. D. Dracoulis, G. J. Lane, I. Ahmad, A. P. Byrne, M. P. Carpenter, P. Chowdhury, S. J. Freeman, N. J. Hammond, R. V. F. Janssens *et al.*, Eur. Phys. J. A **22**, 23 (2004).
[23] M. W. Simon, D. Cline, C. Y. Wu, R. W. Gray, R. Teng, and C. Long, Nucl. Instrum. Methods A **452**, 205 (2000).
[24] M. A. Riley, GAMMASPHERE Users Executive Committee, *"GAMMASPHERE: The beginning . . . 1993–1997"* (1998).
[25] C. Y. Wu, D. Cline, M. W. Simon, R. Teng, K. Vetter, M. P. Carpenter, R. V. F. Janssens, and I. Wiedenhover, Phys. Rev. C **61**, 021305(R) (2000).
[26] C. Y. Wu, D. Cline, M. W. Simon, R. Teng, K. Vetter, M. P. Carpenter, R. V. F. Janssens, and I. Wiedenhover, Phys. Rev. C **68**, 044305 (2003).
[27] D. C. Radford, Nucl. Instrum. Methods A **361**, 297 (1995).

[28] D. Cline, H. S. Gertzman, H. E. Gove, P. M. S. Lesser, and J. J. Schwartz, Nucl. Phys. **A133**, 445 (1969).
[29] D. Cline, Annu. Rev. Nucl. Part. Sci. **36**, 683 (1986).
[30] A. E. Kavka, Ph.D. dissertation, Uppsala University, Uppsala, Sweden (1989).
[31] D. Kotlinski, Ph.D. dissertation, University of Rochester, Rochester (1984).
[32] S. M. Mullins, G. D. Dracoulis, A. P. Byrne, T. R. McGoram, S. Bayer, W. A. Seale, and F. G. Kondev, Phys. Lett. **B393**, 279 (1997); **B400**, 401 (1997).
[33] E. Browne, Nucl. Data Sheets **72**, 221 (1994).
[34] R. B. Firestone, *Table of Isotopes* (Wiley & Sons, New York, 1996), vol. 2, eighth ed.
[35] H. L. Nielsen, K. Wilsky, J. Żylicz, and G. Sørensen, Nucl. Phys. **A93**, 385 (1967).
[36] H. L. Nielsen, K. B. Nielsen, and N. Rud, Phys. Lett. **B27**, 150 (1968).
[37] R. C. de Haan, A. Aprahamian, H. G. Börner, C. Doll, M. Jentschel, A. M. Bruce, and S. R. Lesher, J. Res. Natl. Inst. Stand. Technol. **105**, 125 (2000).
[38] A. Aprahamian, Nucl. Phys. **A731**, 291 (2004).
[39] E. Ngijoi-Yogo, Ph.D. dissertation, University of Massachusetts, Lowell (2004).
[40] E. Ngijoi-Yogo, S. K. Tandel, G. Mukherjee, I. Shestakova, P. Chowdhury, C. Y. Wu, D. Cline, A. B. Hayes, R. Teng, R. M. Clark, *et al*. (2006).
[41] A. M. I. Hague, R. F. Casten, I. Forster, A. Gelberg, R. Rascher, R. Richter, P. von Brentano, G. Barreau, H. G. Borner, S. A. Kerr *et al*., Nucl. Phys. **A455**, 231 (1986).
[42] S. M. Mullins (private communication, 2004).
[43] National Nuclear Data Center online databases (2005), http://www.nndc.bnl.gov.
[44] T. L. Khoo and G. Løvhøiden, Phys. Lett. **B67**, 271 (1977).
[45] T. Czosnyka, D. Cline, and C. Y. Wu, Bull. Am. Phys. Soc. **28**, 745 (1983).
[46] D. Cline and P. M. S. Lesser, Nucl. Instrum. Methods **82**, 291 (1970).
[47] M. B. Smith, P. M. Walker, G. C. Ball, J. J. Carroll, P. E. Garrett, G. Hackman, R. Propri, F. Sarazin, and H. C. Scraggs, Phys. Rev. C **68**, 031302(R) (2003).
[48] R. M. Ronningen, J. H. Hamilton, A. V. Ramayya, L. Varnell, G. Garcia-Bermudez, J. Lange, W. Lourens, L. L. Riedinger, R. L. Robinson, P. H. Stelson *et al*., Phys. Rev. C **15**, 1671 (1977).
[49] N. Pietralla, O. Beck, J. Besserer, P. von Brentano, T. Eckert, R. Fischer, C. Fransen, R.-D. Herzberg, D. Jager, R. V. Jolos *et al*., Nucl. Phys. **A618**, 141 (1997).
[50] C. Y. Wu, W. von Oertzen, D. Cline, and M. W. Guidry, Annu. Rev. Nucl. Part. Sci. **40**, 285 (1990).
[51] E. Browne, Nucl. Data Sheets **54**, 199 (1988).
[52] B. Elbek, *Determination of Nuclear Transition Probabilities by Coulomb Excitation* (Ejnar Munksgaards Forlag, Copenhagen, Denmark, 1963).
[53] C. Y. Wu and D. Cline, Phys. Lett. **B382**, 214 (1996).
[54] X. Wu, A. Aprahamian, J. Castro-Ceron, and C. Baktash, Phys. Lett. **B316**, 235 (1993).
[55] X. Wu, A. Aprahamian, S. M. Fischer, W. Reviol, G. Liu, and J. X. Saladin, Phys. Rev. C **49**, 1837 (1994).
[56] F. W. N. De Boer, P. F. A. Goudsmit, B. J. Meijer, J. C. Kapteyn, J. Konijn, and R. Kamermans, Nucl. Phys. **A263**, 397 (1976).
[57] R. D. Lawson, *Theory of the Nuclear Shell Model* (Oxford University Press, New York, 1980).
[58] P. M. Walker, D. Ward, O. Häusser, H. R. Andrews, and T. Faestermann, Nucl. Phys. **A349**, 1 (1980).
[59] A. O. Macchiavelli and E. Browne, Nucl. Data Sheets **69**, 903 (1993).
[60] E. Browne, Nucl. Data Sheets **68**, 747 (1993).
[61] R. B. Firestone, Nucl. Data Sheets **62**, 101 (1991).
[62] P. Tlustý, D. Vénos, A. Kugler, M. Honusek, and B. Gorski, Phys. Rev. C **48**, 2082 (1993).
[63] N. Boos, F. L. Blanc, M. Krieg, J. Pinard, G. Huber, M. D. Lunney, D. Le Du, R. Meunier, M. Hussonnois, O. Constantinescu *et al*., Phys. Rev. Lett. **72**, 2689 (1994).
[64] E. Lubkiewicz, H. J. Wollersheim, R. Kulessa, C. Briançon, W. Brüchle, O. Constantinescu, M. Dębowski, E. Ditzel, H. Folger, J. Gerl *et al*., Z. Phys. A **355**, 377 (1996).
[65] R. G. Helmer and C. W. Reich, Nucl. Phys. **A114**, 649 (1968).
[66] H. Postma, B. Kastelein, N. Severijns, D. Vandeplassche, J. Vanhaverbeke, L. Vanneste, E. van Walle, J. Wouters, and J. van Klinken, Hyp. Inter. **52**, 79 (1989).
[67] P. A. M. Dirac, *Principles of Quantum Mechanics* (Oxford University Press, London, 1947).
[68] R. F. Casten, *Nuclear Structure from a Simple Perspective* (Oxford University Press, New York, 2000).
[69] E. Schoeters, R. E. Silverans, L. Vanneste, K. Freitag, and H. Hübel, Z. Phys. A **262**, 203 (1975).
[70] N. L. Gjørup, P. M. Walker, G. Sletten, M. A. Bentley, B. Fabricius, and J. F. Sharpey-Schafer, Nucl. Phys. **A582**, 369 (1995).
[71] T. L. Khoo, J. C. Waddington, R. A. O'Neil, Z. Preibisz, D. G. Burke, and M. W. Johns, Phys. Rev. Lett. **28**, 1717 (1972).
[72] K. E. G. Löbner, Phys. Lett. **B26**, 369 (1968).
[73] J. van Klinken, W. Z. Venema, R. V. F. Janssens, and G. T. Emery, Nucl. Phys. **A339**, 189 (1980).
[74] P. Ring and P. Schuck, *The Nuclear Many-Body Problem* (Springer-Verlag, New York, 1980).
[75] T. L. Khoo (private communication, 2006).
[76] T. Bengtsson, R. A. Broglia, E. Vigezzi, F. Barranco, F. Dönau, and Jing-ye Zhang, Phys. Rev. Lett. **62**, 2448 (1989).
[77] D. Cline, A. B. Hayes, and C. Y. Wu, J. Mod. Opt. **52**, 2411 (2005).
[78] C. B. Collins, F. Davanloo, M. C. Iosif, R. Dussart, J. M. Hicks, S. A. Karamian, C. A. Ur, I. I. Popescu, V. I. Kirischuk, J. J. Carroll *et al*., Phys. Rev. Lett. **82**, 695 (1999).
[79] W. Z. Venema, R. V. F. Janssens, J. van Klinken, and G. T. Emery, Nucl. Instrum. Methods A **201**, 531 (1982).